Broadband Predictions of Optimized Proprotors in Axial Forward Flight

Joshua D. Blake,* Christopher S. Thurman,† Nikolas S. Zawodny,‡ and Leonard V. Lopes§
NASA Langley Research Center, Hampton, VA, 23681

A low-fidelity toolchain was used to predict broadband self-noise trends for three proprotors in axial flight: a baseline (C24ND) and two acoustically constrained proprotors (OPT-III and COPR-3). Rotor loads were predicted with the ANOPP Propeller Analysis System (PAS) and self-noise was predicted with the semiempirical method of Brooks, Pope, and Marcolini (BPM) implemented in the ANOPP2 Self-Noise Internal Functional Module (ASNIFM). Comparisons to experimental data revealed that trends for turbulent boundary layer trailing edge (TBL-TE) noise could be modeled across several flight conditions by increasing the boundary layer thicknesses via the trip setting. Since the Mach number range of the BPM method is exceeded in these predictions, a dependence of boundary layer displacement thickness on blade station Mach number was suggested as a possible reason for needing to model thicker boundary layers, suggesting that the TBL-TE model needs to be developed further. Bluntness vortex shedding noise (BVS) predictions required tuning the trailing edge thickness and trailing edge closure angle for each flight condition to match experimental trends, demonstrating that the BVS noise model is incomplete and that BVS noise may vary with the angle of attack. This study indicates that the BPM self-noise method needs to be improved, which will lead to more accurate broadband predictions.

I. Introduction

The rapidly growing Advanced Air Mobility (AAM) industry is generating a variety of new vehicle concepts and designs. Urban Air Mobility (UAM), a subset of AAM operations, refers to the transport of passengers and cargo over densely populated areas. UAM vehicles will likely be powered by electric motors and operate at ranges of around 120 km below altitudes of 1,000 meters [1, 2]. Vehicles may employ a combination of propellers, rotors, or proprotors and may be capable of transitioning between VTOL and axial forward flight. Given the intended operational space, a major focus and challenge for UAM vehicle design is quiet flight throughout the operational envelope. Minimizing UAM vehicle noise will be a key driver to community acceptance of these new modes of transportation.

Propeller- and rotor-driven vehicles have many component noise sources, including the rotor, motor, airframe interactions, rotor-to-rotor interactions, and vibrational noise. The major contributor to noise on these vehicles is the rotor, which emits noise that is both periodic (i.e., tonal noise) and stochastic (i.e., broadband noise) in nature. Tonal noise is dependent on the rotor rotational rate and produces tones at the fundamental blade passage frequency (BPF) and harmonics, which tend to occur at low frequencies. Broadband noise is related to unsteady fluctuations from turbulence and shed vortices, which generate noise over a range of mid-to-high frequencies.

Tonal noise has typically been the major noise source for propellers in axial flight. Conventional tube-and-wing aircraft propellers operate at rotational speeds corresponding to tip Mach numbers in the range of 0.7 and higher, where low-frequency tonal noise dominates the radiated noise. In contrast, UAM proprotors are expected to operate at tip Mach numbers in the range of 0.5 or lower [3] and at reduced rotational speeds [2], especially in forward flight. As the rotational rate decreases, the proprotor tones shift lower in frequency. Given the nature of human perception, which is most sensitive to mid frequencies and less sensitive to low frequencies, the majority of tonal noise from UAM propellers and proprotors will be effectively attenuated at lower rotational speeds. Broadband noise will then likely fall within the range of frequencies most annoying to a human observer (1 to 5 kHz), and proprotor self-noise is expected to contribute significantly to the total UAM system noise [2].

*Research Aerospace Engineer, Aeroacoustics Branch, AIAA Member; joshua.d.blake@nasa.gov
†Research Aerospace Engineer, Aeroacoustics Branch, AIAA Member; christopher.thurman@nasa.gov
‡Senior Research Aerospace Engineer, Aeroacoustics Branch, AIAA Member; nikolas.s.zawodny@nasa.gov
§Senior Research Aerospace Engineer, Aeroacoustics Branch, AIAA Member; leonard.v.lopes@nasa.gov

Depending on the vehicle configuration and proprotor operational conditions, broadband rotor noise can be a significant contributor to UAM vehicle noise. For instance, the use of electric or hybrid-electric propulsion [2] will reduce motor noise and increase the significance of broadband proprotor noise. Recent tests by Joby Aviation [4, 5] showed that in forward flight, when accounting for human perception, the noise emitted by Joby's electric vertical takeoff and landing (eVTOL) vehicle was dominated by broadband content in the frequency range of 2 to 4 kHz due to the low rotational speed of the proprotors. Given the possibility that broadband noise may be a significant noise source for UAM vehicles, broadband noise predictions are needed for proprotors operating in both hover and forward flight.

Due to the abundance of unique vehicle configurations, the ability to inform the design process early on with noise predictions is key. Gradient-based design frameworks, such as OpenMDAO [6], can take advantage of low-fidelity aerodynamic tools like blade element momentum theory (BEMT) [7] and noise prediction tools like the second-generation Aircraft NOise Prediction Program (ANOPP2) [8] to guide toward acoustically optimal designs. These tools have been applied to the X-57 propeller, showing that design optimization can be used to reduce tonal noise with minimal aerodynamic performance penalty [9]. Due to its relative insignificance for traditional propeller-driven aircraft, broadband noise has typically not been considered in acoustic-constrained optimization. However, as design optimization tools reduce rotation rate to minimize tonal noise, the relative significance of broadband noise will increase. By demonstrating that broadband predictions can be made with a sufficient level of accuracy with low-fidelity tools, broadband noise could potentially be included in rotor and vehicle design.

Optimization-based design tools require quick proprotor noise predictions to inform design trends. A low-fidelity tonal and broadband noise prediction toolchain has been applied to small unmanned aircraft systems (sUAS) rotors in hover and edgewise forward flight [10, 11] and to an ideally twisted rotor in hover [12, 13] with good agreement. However, this type of low-fidelity toolchain has not been widely applied to propellers in axial forward flight. For vehicle design optimization, these low-fidelity tools need to predict proprotor noise accurately in all vehicle operating conditions, including axial flight.

This work focuses on using a similar low-fidelity analysis toolchain to Refs. [10–13] to predict broadband self-noise in axial forward flight for isolated proprotors, which is an important first step in evaluating the total vehicle noise. The predictions employ a suite of publicly available aerodynamic and aeroacoustic tools, including ANOPP-PAS [14] for predicting aerodynamic loads and the induced rotor inflow. The ANOPP2 Self Noise Internal Functional Module (ASNIFM), accessed through a command line interface called the ANOPP2 Broadband Acoustic Rotor Tool (ABART), will be used for broadband predictions [8]. ASNIFM uses the Brooks, Pope, and Marcolini (BPM) method for self-noise predictions [15]. Although several methods exist for predicting airfoil self-noise [16], BPM is semiempirical and is therefore a simple and quick approach to predicting broadband noise from airfoils. Exercising these tools will provide some insight into their applicability for UAM proprotor noise predictions.

A baseline and two acoustically optimized proprotors are compared to experimental results from a recently conducted study at the NASA Langley Low Speed Aeroacoustic Wind Tunnel (LSAWT) facility [17]. The goal of this current study is to identify where the broadband noise models fail or where the level of fidelity of the employed methods is not sufficient for the task, as well as to identify best practices for model parameters. Evaluating the shortcomings of low-fidelity analysis tools gives confidence in applying these tools in acoustic optimization problems. Making quick and sufficiently accurate predictions of broadband noise for proprotors in several configurations is key to enabling low-noise design early in a vehicle design optimization loop, which should help reduce barriers to community acceptance.

The outline of this paper is as follows. The technical approach of this research is described, including the proprotor geometries and experimental data processing. Additionally, the prediction methodology and several known model shortcomings are detailed. Predictions are presented for each proprotor, focusing on the model parameters that influence two broadband self-noise sources. Areas in which the models need to be improved are discussed, followed by considerations for design optimization using broadband predictions. Finally, conclusions and future work are discussed.

II. Technical Approach

The geometries of the proprotors in the experimental test and processing of the experimental data are briefly discussed in this section, as well as the broadband noise prediction methods and setup. Additionally, limitations of the BPM method are discussed as they relate to the data set in question.

A. Proprotor Geometry

Several three-bladed proprotors were tested at the LSAWT facility: the C24ND, OPT-III, and the COPR-3, shown in Fig. 1. These three proprotors were the result of a design optimization campaign intended to generate acoustically

constrained proprotors using both low- and high-fidelity methods. For a given target thrust, a baseline proprotor (the C24ND) was used as an initial geometry for the optimization process. While meeting the design thrust, the proprotor was first optimized for maximum efficiency. Then a constraint was added to minimize sideline tonal noise, resulting in a trade-off between efficiency and noise. For additional details, see Refs. [9, 17, 18].

The C24ND is a helically twisted proprotor designed as a propeller for a more conventional single-engine airplane and thus operates at a faster rotation rate with a design M_{tip} = 0.667. The OPT-III proprotor is the result of applying a computational fluid dynamics-based design optimization framework to minimize tonal noise. The airfoil shape, twist, chord distribution, and rotation rate were modified in the optimization process, but changes were limited by computational grid deformation issues [18], so the OPT-III blade shape does not appear significantly different from the C24ND. The OPT-III proprotor is designed to operate at M_{tip} = 0.619. The COPR-3 is the result of applying the OpenMDAO optimization tool chain to the C24ND geometry to produce an acoustically optimized proprotor that maintains aerodynamic performance while minimizing tonal noise [9]. The optimizer reduced the rotation rate to M_{tip} = 0.343 and shifted the blade thickness inboard, yielding results similar to optimization results for a small single-engine type aircraft [19].

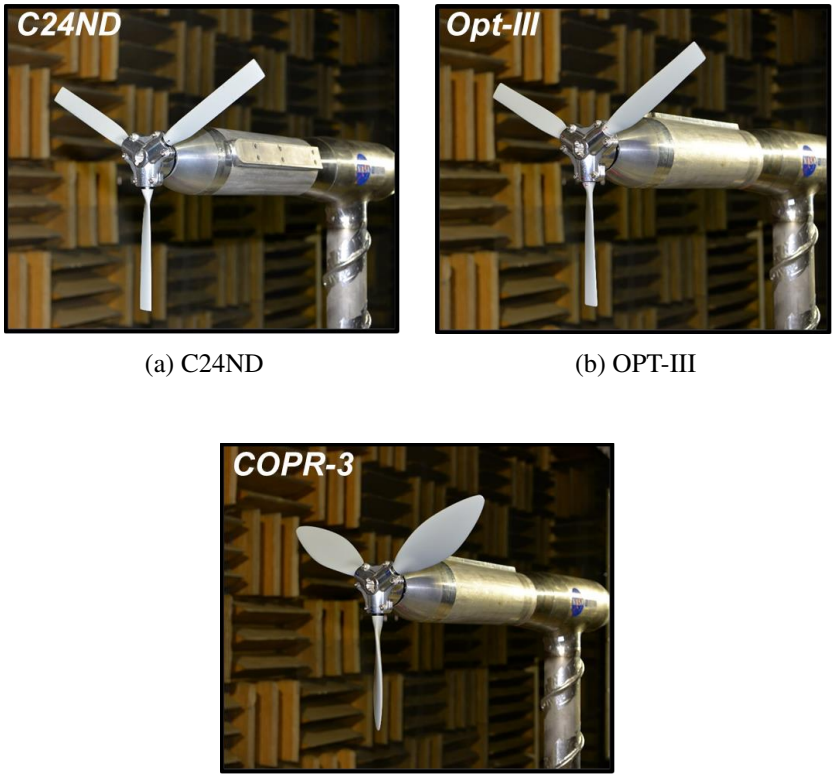

(a) C24ND (b) OPT-III

(c) COPR-3

Fig. 1 Photographs of the three-bladed proprotors tested in LSAWT [17, Source: NASA].

The contrast of rotation rates makes these proprotors ideal for investigating the range of applicability of the tool chain since the C24ND and OPT-III blades represent conventional propellers and the COPR-3 blade represents a low tonal noise design. The C24ND and COPR-3 are constructed with nominally NACA 0012 airfoils because this airfoil is well understood and because the toolchain, especially the BPM method, was designed around NACA 0012 airfoils. The OPT-III airfoils were allowed to deviate from the NACA 0012 shape but did not change significantly. The C24ND and COPR-3 proprotors both have a diameter of 0.6096 meters, and the OPT-III proprotor has a reduced diameter of 0.6002 meters. Additional details of the design of each proprotor can be found in the NASA Technical Memorandum (TM) documenting the test campaign [17].

B. Experimental Data Processing

The C24ND, OPT-III, and COPR-3 proprotors were tested at several tunnel speeds in the LSAWT test campaign. Additionally, the OPT-III and COPR-3 proprotors were operated at several rotational rates. Far-field noise was recorded by a linear array of microphones located 3.54 meters (approximately 12R) from the proprotors as shown in Fig. 2. Since these proprotors are model scale, the recorded frequencies extended from 50 Hz to 80 kHz. The experimental data were corrected for atmospheric attenuation and for propagation through the shear layer of the LSAWT, assuming a point source at the proprotor hub. The broadband noise is extracted by removing the tonal peaks through a periodic averaging process. The NASA TM can be consulted for additional data processing details [17]. The experimental data included in this paper are available, and interested parties should contact Leonard Lopes for additional details (leonard.v.lopes@nasa.gov).

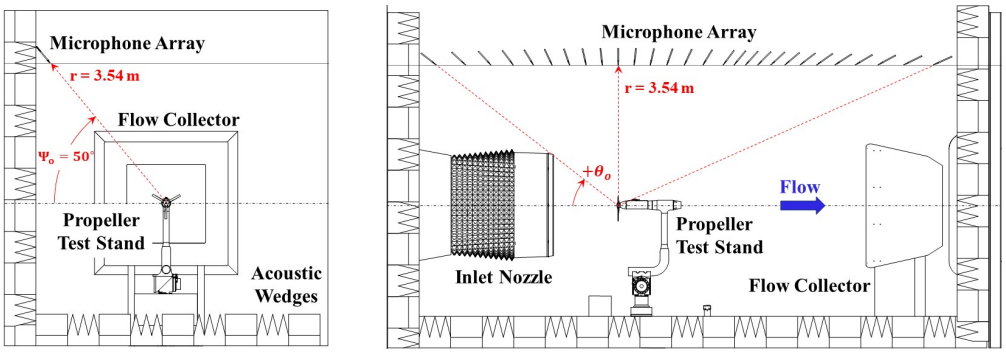

(a) Front View (b) Side View

Fig. 2 Front and side views of LSAWT and the microphone array.

C. Computational Methods

Isolated proprotors generate several broadband noise sources, including self-noise, blade-wake interaction (BWI), and turbulence ingestion noise (TIN). The focus of the broadband noise predictions in this work is on self-noise, so BWI and TIN are not considered, nor are any tonal noise sources. Self-noise can be further broken down into its components and includes turbulent boundary layer trailing edge (TBL-TE) noise from both the pressure and suction side of the proprotor blade, trailing edge noise due to separation and stall, laminar boundary layer vortex shedding noise (LBL-VS), bluntness vortex shedding noise (BVS), and tip vortex formation noise [15].

An example of the relative importance of each of the broadband sources from the BPM method are shown in Fig. 3 using the COPR-3 proprotor operating at $M_\infty = 0.111$ and $M_{tip} = 0.343$. All components except LBL-VS are shown in Fig. 3 (a). Predictions in this work do not include LBL-VS self-noise because the BPM method does not always predict the correct frequencies or amplitudes for LBL-VS noise [12, 13]. The summation of the TBL-TE suction (blue triangles), pressure (red stars), and separation (orange triangles) is the total TBL-TE noise, which is represented in Fig. 3 (b) by green triangles. Figure 3 (b) shows only the total TBL-TE and BVS components and the total combined prediction (gray circles), demonstrating that total TBL-TE and bluntness noise are the two dominant noise sources for the flight conditions shown.

Proprotor loads and aerodynamic quantities, which are necessary for broadband noise predictions, are computed by the ANOPP Propeller Analysis System (PAS) [14], a BEMT solver for axial propeller flight. Using low-fidelity aerodynamic methods like BEMT gives a quick yet fairly accurate prediction for radially varying proprotor loads and aerodynamic sectional properties, including the induced axial and tangential velocities at the proprotor disk and the effective angles of attack. The PAS code calculates airfoil tables for blade stations using potential theory and elliptical transformations for general airfoil shape [20, 21]. Airfoil stall is not explicitly modeled in PAS but the sectional lift and drag coefficients can be limited to a specified angle of attack. Tip loss effects can also be included in the prediction of proprotor loads.

Broadband predictions are performed using the BPM method [15], which is implemented in a rotating blade framework in ASNIFM. The command line interface ABART is used to easily call ASNIFM for a proprotor. Inputs to ASNIFM/ABART include the proprotor operating conditions (i.e., rotation rate and forward velocity), as well as the

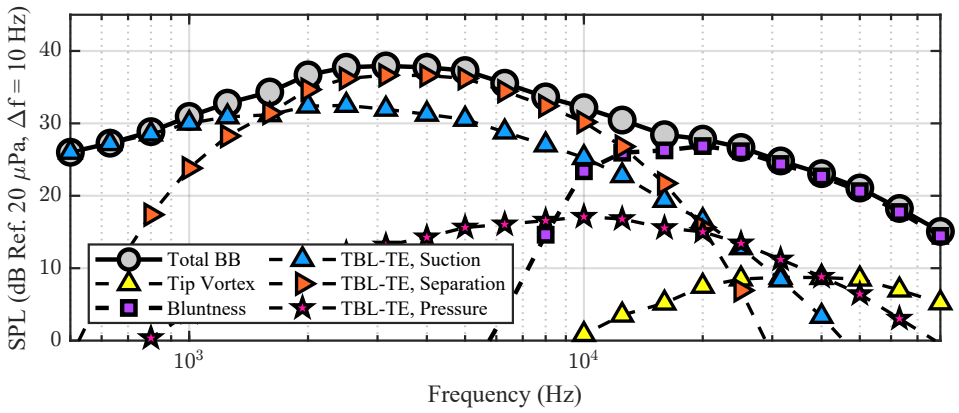

(a) All Broadband Noise Components Except LBL-VS

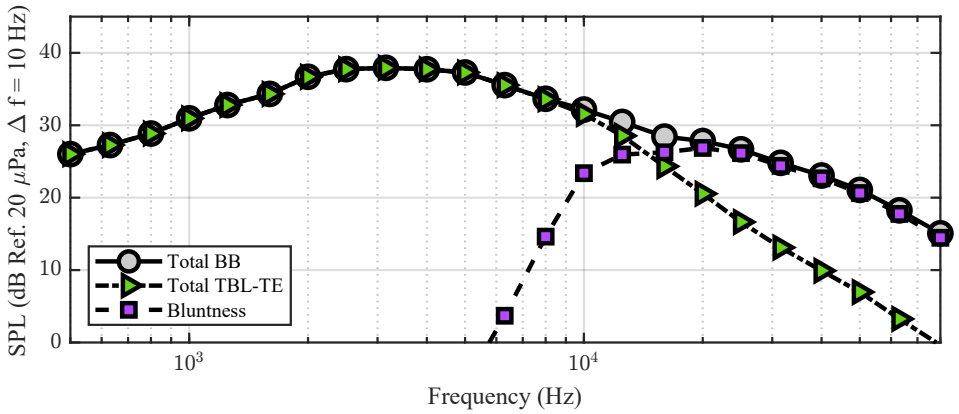

(b) Only TBL-TE and BVS Noise Components

Fig. 3 Broadband predictions with a source component breakdown using the COPR-3 proprotor operating at $M_\infty = 0.111$ and $M_{tip} = 0.343$.

twist, local effective angle of attack (α), and local induced velocities that are computed by PAS at each blade section. There are several tuning parameters including a boundary layer trip setting, trailing edge thickness, and trailing edge closure angle, all of which can be varied along a blade span. Ideally, the choice of these parameters should exactly match the experimental setup since the predictions are highly sensitive to the boundary layer properties [12]. However, the choice of these parameters is often somewhat arbitrary due to the fact that the trailing edge geometry and boundary layer properties are difficult to measure for small rotors [12]. Other options include the ability to model a square or rounded tip, which influences the tip vortex formation noise. A Reynolds number limit can also be used to suppress LBL-VS noise for small blades [12, 13].

D. Prediction Settings and Limitations

For both aerodynamics and acoustics, the blade sections were assumed to have an NACA 0012 airfoil profile for all blade stations (note that this is a modeling simplification for the OPT-III proprotor, which did not have NACA 0012 airfoil profiles). The C24ND blade was discretized into 39 stations, the OPT-III blade into 35 stations, and the COPR-3 into 31 stations. The number of stations varied from blade to blade based on the computational representation of each blade geometry that was available. All blades had stations clustered near the tip with the minimum airfoil station at $r/R = 0.2$ to $r/R = 0.25$, depending on the underlying geometry discretization.

For aerodynamic loads, airfoil tables were generated by PAS with angles of attack limited to $\pm 12^\circ$ and up to Mach 0.7. At each proprotor design operating condition, a target thrust of 107 N was matched in PAS for each proprotor by slightly adjusting the collective blade pitch, with each blade needing less than a degree of root collective adjustment. A uniform freestream inflow was applied equally across the proprotor disk at a zero-degree incidence to the proprotor axis.

The calculated induced inflow velocities were observed to vary radially as is expected with BEMT. Tip loss effects were not included in the proprotor loads, which is standard practice for broadband noise predictions [11, 12] due to PAS predicting large nonphysical angles of attack at the tip, resulting in spurious broadband noise predictions. Airfoil section properties, such as the local angles of attack and induced velocities, were then extracted and used as inputs to ASNIFM to perform broadband noise predictions.

All broadband predictions were computed as third-octave band data from the BPM method in ASNIFM and converted to 10 Hz narrowband representations, assuming equal acoustic energy, for comparison to experimental data. The array of acoustic observers for noise prediction loosely corresponds to a linear array of microphones that approximate the LSAWT microphone array (see Fig. 2). For this investigation, a single observer was studied at 45° below the rotor plane: $\theta = 135°$ and r = 5.00 m.

Settings were investigated for three BPM parameters: trip setting, trailing edge angle, and trailing edge thickness. Each parameter was specified at radial stations along the blade. The trip setting adjusts the boundary layer trip and modifies boundary layer thicknesses. The airfoil trailing edge thickness and trailing edge angle modify bluntness noise.

The BPM method has default values that were not varied for these predictions. The angle for tip vortex formation noise was set to 1.1°, and tip vortex noise is included in the total broadband predictions. Brooks, Pope, and Marcolini [15] theorized that bluntness noise is dependent on Mach number and proposed a Mach number limit of 0.45 for BVS noise [15] above which no BVS should be predicted. This limit is implemented in ASNIFM and in these predictions. LBL-VS noise is not included in the broadband predictions since this mechanism is still difficult to model correctly [12, 22], but some of the experimental data investigated here may contain LBL-VS noise.

The BPM method was created from 2D and 3D airfoil experiments and has some notable limitations for broadband predictions. First, the BPM method only models the self-noise for a symmetrical NACA 0012 airfoil for Reynolds numbers up to 1.5×10^6 and Mach numbers up to 0.208. The Mach number limit is a concern for the proprotors in this study since the tip Mach numbers are greater than this limit. Figure 4 shows each of the three proprotors and their corresponding tip Mach numbers. The portions of the blade that fall within the limits on which BPM was built are shown. Notably, the outboard portions of each blade (where the majority of broadband noise is generated) fall outside the range for which the BPM method was designed. This raises the question as to how the BPM method performs outside these limits.

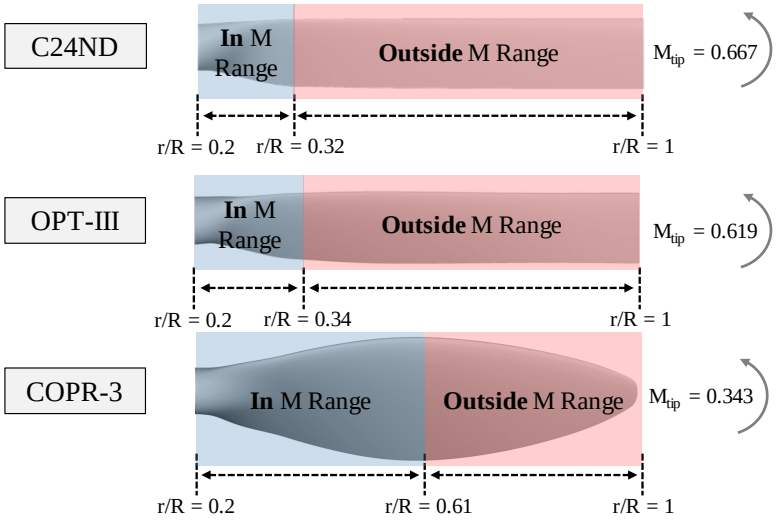

Fig. 4 Portions of the three proprotor blades inside and outside the range of the Mach number limits of the BPM method.

Additionally, most of the BPM noise sources are based on the displacement thicknesses of the boundary layer at the trailing edge, δ^*. Since boundary layer quantities are difficult to measure, the BPM method provides empirical curve fits to boundary layer displacement thickness as a function of sectional aerodynamic properties. These models of boundary layer thickness are for only two boundary layer states: untripped and fully (aggressively) tripped. If the

boundary layer thicknesses are not predicted correctly, then the BPM model will not predict the broadband noise trends correctly. Essentially, the accuracy of the BPM predictions hinges on predicting the boundary layer correctly but is limited by the data on which the method was built. An additional limitation of the BPM method is that some of the data were sparse at mid-range angles of attack in the 6° to 12° range. Given the semiempirical nature of the BPM method and the limited Mach number range and angle of attack sparseness, this work seeks to investigate how these limitations influence broadband noise predictions.

III. Broadband Model Parameter Investigation

From the predictions in Fig. 3, the two main components of broadband noise for the C24ND, OPT-III, and COPR-3 proprotors in axial forward flight are expected to be TBL-TE noise and BVS noise. TBL-TE is noise due to turbulence passing the trailing edge, and BVS is noise due to vortices shed from a blunt trailing edge.

In the following section, total TBL-TE noise (the combination of suction, pressure, and separation/stall noise sources) and bluntness (BVS) noise are investigated by varying their corresponding BPM model parameters. First, the effect of boundary layer trip on the TBL-TE noise is studied, followed by the effect of trailing edge geometry on BVS noise (also referred to as bluntness noise). The goal is to identify the model parameters leading to the best predictions for axial forward flight and to investigate any discrepancies between the predictions and experimental data due to the limitations (i.e., Mach number) of the semiempirical BPM model.

A. Trailing Edge Noise

The trailing edge (total TBL-TE) noise models in the BPM method take in aerodynamic quantities (local Reynolds number, Mach, and angle of attack) and geometric quantities (chord and spanwise section length). The only remaining model parameter is the trip setting, a quantity that is 0.0 for an untripped boundary layer and 1.0 for a fully tripped boundary layer. This section investigates the influence of trip setting on the boundary layer thicknesses and on the resulting total TBL-TE noise predictions for the C24ND, OPT-III and COPR-3 proprotors, concluding with a brief look at how the boundary layer thicknesses may vary with Mach number.

1. Trip Setting and Boundary Layer Thicknesses

The boundary layer trip setting (untripped or fully tripped) in ASNIFM can be conceptualized as a parameter that modifies the boundary layer thicknesses at the trailing edge, specifically, the displacement thickness, δ^*. The value of δ^* modifies the frequency and amplitude of the peak TBL-TE noise. The trip setting can therefore be adjusted to tune the boundary layer thicknesses and TBL-TE noise to a desired result.

Figure 5 shows the suction-side displacement normalized by chord, δ_s^*/c, for an airfoil at a Reynolds number of 500,000. The trip settings plotted are untripped, moderately tripped, and fully tripped. These three curves represent trip settings of 0.0, 0.5, and 1.0 in ASNIFM. The untripped and fully tripped curves are generated using the BPM method. Moderately tripped is simply an average of the untripped and fully tripped values for δ^* computed after δ^* is corrected for α. Adjusting δ^* changes both the frequency and amplitude of the peak TBL-TE noise. Turning the trip setting into a scalar, rather than a binary setting, allows indirect study of the influence of boundary layer size on the radiated TBL-TE noise.

2. Total TBL-TE Noise For Varying Tunnel Speeds

Predictions using ASNIFM were performed for each trip setting (untripped, moderately tripped, and fully tripped). A constant tip speed was held while the tunnel speeds were varied for all three proprotors. The tip speed for each proprotor was the design tip speed, but the tunnel speeds were identical across all proprotors. The frequency and ranges of plots in this section are adjusted to highlight the regions of maximum TBL-TE noise for each proprotor. These plots provide a wide range of conditions over which the TBL-TE predictions can be evaluated.

Predictions were calculated for the OPT-III proprotor at M_{tip} = 0.619 and are shown by the black lines with colored symbols in Fig. 6 (a) for untripped, (b) for moderately tripped, and (c) for fully tripped boundary layers. Experimental data from four corresponding tunnel speeds (Mach = 0.075, 0.090, 0.111, and 0.125) are plotted in the colored lines. In the experimental data, there is a hump at 3 kHz but it is unclear if this is TBL-TE noise or some additional source like hub noise that the BPM method cannot predict. Until additional data can be gathered, it is assumed that the TBL-TE noise is found at 3 kHz and above. Tonal spikes observed in the experimental data around 3 kHz could be motor noise, which the BPM method also cannot predict.

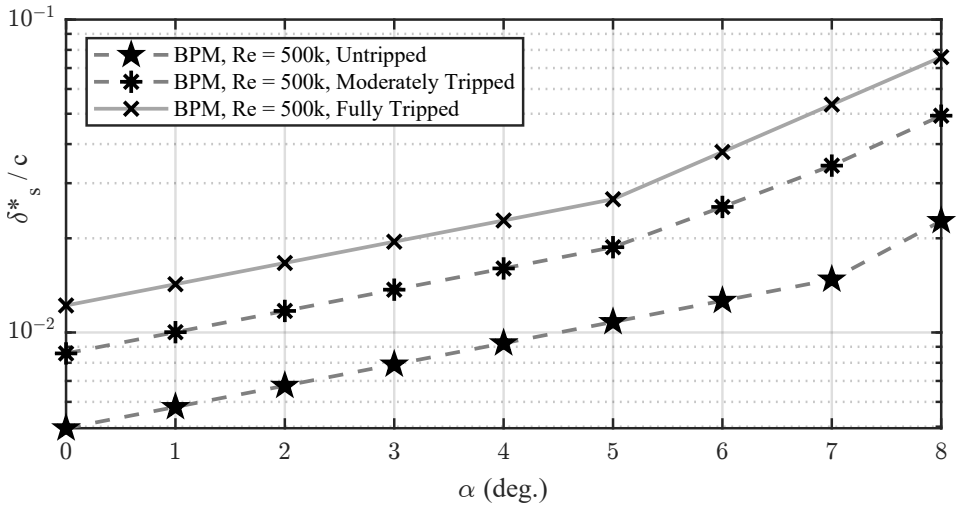

Fig. 5 Increase in the suction side boundary layer displacement thickness, δ^*_s, with increasing angle of attack and varying trip for a chord-based Reynolds number of 500,000.

The predictions in Fig. 6 follow the expected trend, that increasing the trip setting increases the peak TBL-TE amplitude but lowers the peak frequency. The TBL-TE predictions roll off at high frequencies, where it is expected that BVS noise will dominate when included in the predictions. Roll-off also occurs at the low frequencies, where the measured noise transitions to other non-self-noise noise sources. The untripped setting underpredicts amplitude, and the curve of the spectra does not match, indicating that the correct frequency trends are not predicted. The fully tripped setting agrees well for the two fastest tunnel speeds but overpredicts amplitude for the lowest frequencies at the slowest speeds. The moderately tripped setting shows the best agreement in amplitude and frequency over the four tunnel speeds, but still shows some differences in amplitude at the peak TBL-TE frequencies.

Looking at the angles of attack from PAS for the four predictions (Fig. 7), the slowest tunnel speed (M_∞ = 0.075) is likely experiencing stall on the inboard sections of the blade. Although PAS does not model stall, the BPM method does model separation or stall noise if the effective angle of attack at a blade station is large enough. This is reflected in the corresponding experimental data in Fig. 6 by an increase in TBL-TE and separation/stall noise from 3 kHz to 10 kHz for the slowest tunnel speed.

Experimental data and broadband predictions for the COPR-3 proprotor are shown in Fig. 8. The fastest tunnel speed (M_∞ = 0.125) was not included because the measured proprotor noise was not sufficiently above the tunnel background noise and comparing to predictions would not have yielded useful information. Instead, the tunnel background noise for M_∞ = 0.111 is shown to indicate that there is still a low signal-to-noise ratio even for this tunnel speed. The low rotation rate of the COPR-3 proprotor (nearly half of the OPT-III) shifts the TBL-TE noise peak to lower frequencies than the TBL-TE peak for the OPT-III proprotor. Again, roll-off is observed above 5 kHz where bluntness noise is expected to contribute to the total proprotor noise.

The untripped, moderately tripped, and fully tripped predictions in Fig. 8 again follow the same trend that increasing the trip shifts the peak total TBL-TE noise. The untripped setting again fails to match the peak TBL-TE noise, instead predicting it to occur at higher frequencies and lower amplitudes. Fully tripped predictions agree well at the two slowest tunnel speeds, but overpredict the amplitude for the fastest tunnel speed (M_∞ = 0.111). The moderately tripped setting again gives the best predictions for total TBL-TE over all tunnel speeds. Again, there is a spectral hump below 1 kHz in the slowest tunnel speeds that the BPM method cannot predict, which could be root or stall noise.

Compared to the OPT-III proprotor (see Fig. 7), the angle of attack distribution shown in Fig. 9 for the COPR-3 proprotor is relatively constant. The angles of attack for the design condition (M_∞ = 0.111) correspond to the peak lift-to-drag ratio for an NACA 0012 airfoil at those flight conditions, which indicates that the COPR-3 propeller represents a minimum induced loss design. The angles of attack for the two slowest tunnel speeds indicate that most sections are at or near stall, which can be observed by the increase in amplitude at the peak TBL-TE noise in the experimental data for these two speeds (Fig. 8).

Predictions are compared to experimental data for the C24ND proprotor at M_{tip} = 0.667 in Fig. 10 (a) for untripped, (b) for moderately tripped, and (c) for fully tripped settings. Tonal spikes around 10 kHz could be due to motor noise that

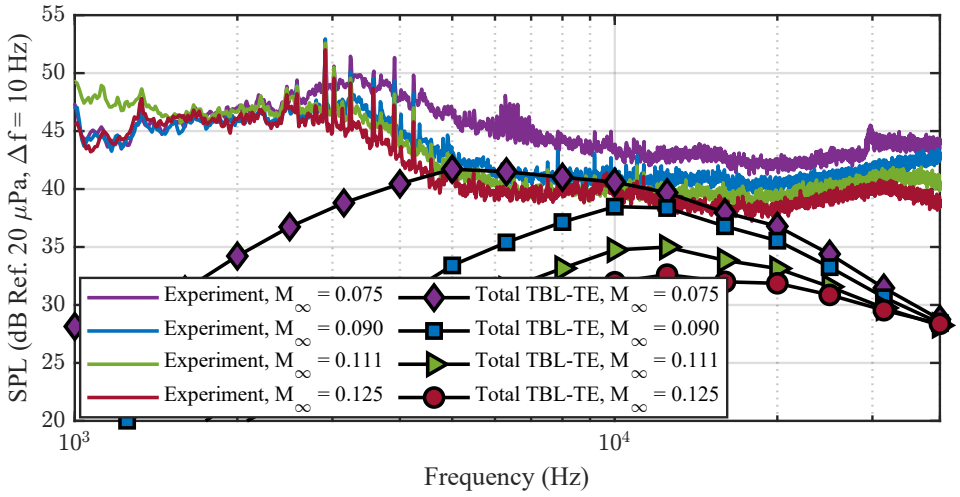

(a) Untripped Boundary Layer

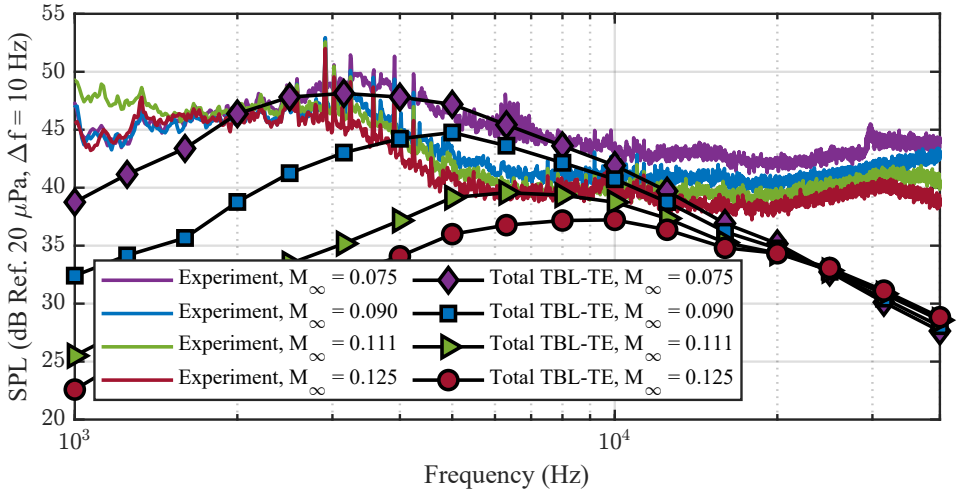

(b) Moderately Tripped Boundary Layer

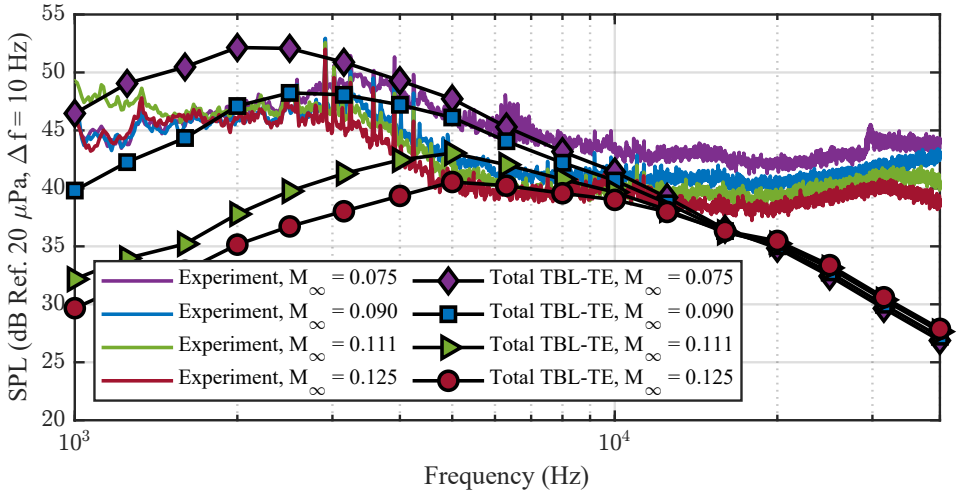

(c) Fully Tripped Boundary Layer

Fig. 6 The effect of varying freestream velocity and boundary layer trip setting on Total TBL-TE predictions for the OPT-III proprotor operating at M_{tip} = 0.619. Experimental narrowband (10 Hz) data are shown by solid colored lines. Predictions are shown in black lines with symbols.

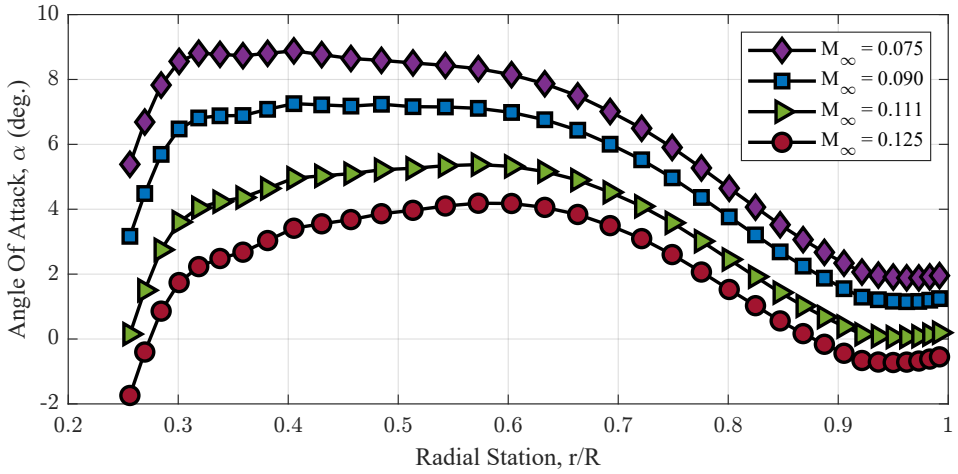

Fig. 7 Angles of attack predicted by PAS for the OPT-III proprotor at M_{tip} 0.619 and varying tunnel speeds (M_∞).

the BPM method cannot predict. For all trip settings and tunnel speeds, the model underpredicts the experimental data. The frequency content is not well predicted by any trip setting either. The moderately tripped case does approximate the correct spectral shape for the peak TBL-TE noise in the 7 kHz to 13 kHz range, but the amplitude is underpredicted by 5 dB. The reason for this underprediction is still unknown, but Section III.A.3 suggests that the boundary layer thicknesses may not be predicted well by the BPM case for the high tip Mach number of the C24ND proprotor.

For all four tunnel speeds in Fig. 10, a hump can be observed in the experimental data at 2–3 kHz that the BPM method is not predicting. The amplitude of the hump is more pronounced at the slowest two tunnel speeds where the angles of attack (Fig. 11) show that the inboard blade stations may be stalled. For the two fastest tunnel speeds, the angles of attack are moderate and not near stall. However, there is still additional noise at lower frequencies that the BPM method is not predicting. It is likely for the C24ND proprotor that there is additional stall noise from the hub, root, or inboard blade stations.

The inboard blade stations near the root are not aerodynamically significant since they do not carry much of the thrust load nor do they experience high effective velocities. These inboard blade stations are more likely to have larger thickness-to-chord ratios and may even have elliptical or circular profiles as the blade lofts into the root shank. For instance, the transition to a circular root on the C24ND blade begins around r/R = 0.352. Inboard stations might be prone to stall or separation at lower angles of attack than the outer blade stations due to thicker airfoil shapes. Increased airfoil thickness and possible stall suggests that the trailing edge boundary layer experienced by an airfoil at these sections could be significantly larger than for an NACA 0012 airfoil section out near the tip. This leads to the hypothesis that the root sections could be responsible for significant trailing edge or stall/separation broadband noise for the C24ND proprotor.

The 2–3 kHz hump in the experimental data in Fig. 10 could come from stalled flow at the root. It is possible that in the experiment, the transition of the C24ND blade from an airfoil cross section to a cylinder near the root generated an adverse pressure gradient that induced separation or stall. The root transition is not modeled in the current prediction setup, which is one possible explanation for why the 2–3 kHz hump is not observed in Fig. 10.

As a way to approximately model noise due to root stall, the angles of attack input to ASNIFM were increased to 9° for the first 5 blade stations, up to r/R = 0.352, to model a possible increase in δ^* that would accompany flow separation or stall. Increasing α also increases δ^* and shifts the peak total TBL-TE noise to lower frequencies and higher amplitudes, much like increasing the trip setting in the previous section. Figure 12 shows the original TBL-TE prediction (green triangles) and the TLB-TE prediction with increased root angles of attack (orange squares). The prediction with increased root α shows an additional hump around frequencies of 2 kHz. This illustrates that the spectral hump in the experiments can be approximately matched if δ^* is increased for the inboard blade stations, which would occur if those stations were experiencing flow separation or stall. However, this is simply a thought experiment and does not prove the existence of root stall noise. To do so would require additional tests with advanced source localization techniques or high-fidelity simulations.

All three proprotor blades were made of carbon fiber and had a smooth paint layer applied, so it was assumed that

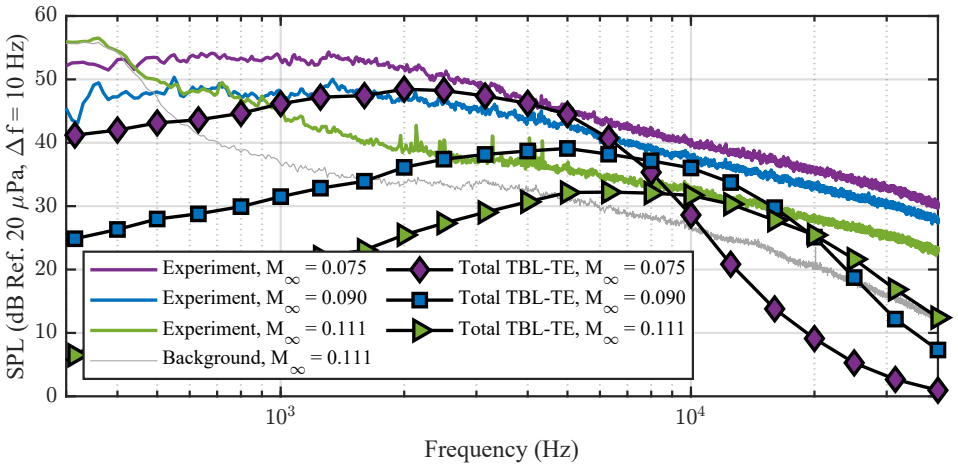

(a) Untripped Boundary Layer

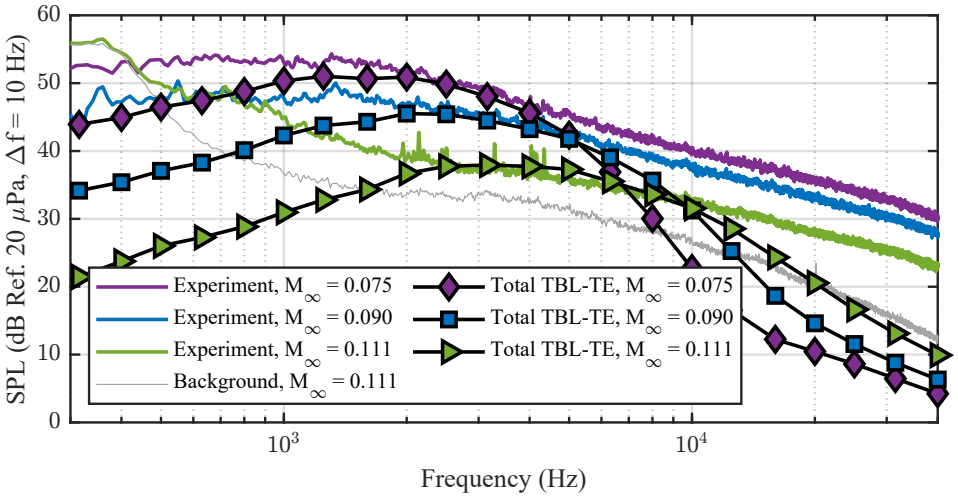

(b) Moderately Tripped Boundary Layer

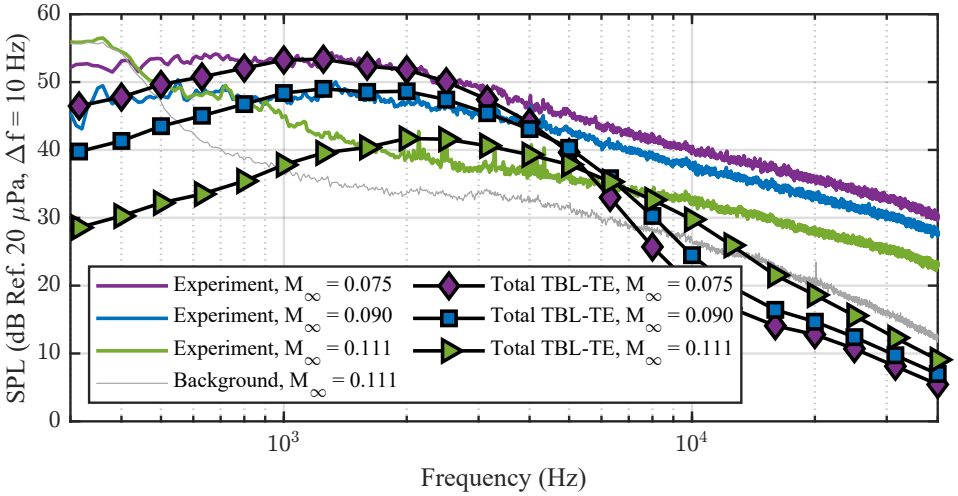

(c) Fully Tripped Boundary Layer

Fig. 8 The effect of varying freestream velocity and boundary layer trip setting on Total TBL-TE predictions for the COPR-3 proprotor operating at M_{tip} = 0.343. Experimental narrowband (10 Hz) data are shown by solid colored lines. Predictions are shown in black lines with symbols.

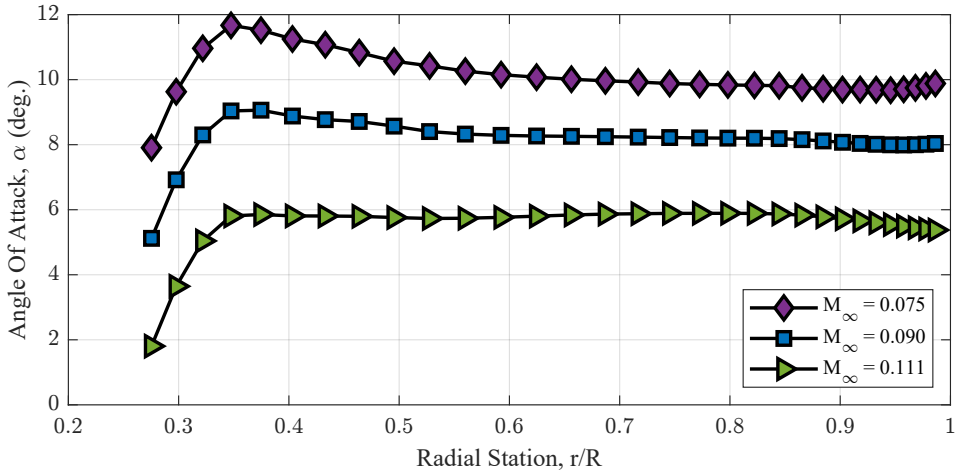

Fig. 9 Angles of attack predicted by PAS for the COPR-3 proprotor at M_{tip} = 0.343 and varying tunnel speeds (M_∞).

they were operating with untripped or freely transitioning boundary layers. Therefore, it is reasonable to assume that the untripped boundary layer setting in BPM should be used for predictions. However, the predictions in this section suggest that the moderately tripped setting or fully tripped setting gives the best results for TBL-TE noise, giving rise to the question: why does the trip setting have to be increased? Section III.A.3 investigates this issue further, suggesting that the issue is the Mach number deficiency of the BPM method. The moderately tripped setting can be considered a model for simply increasing the boundary layer thicknesses, δ^*, modeled in BPM without using the fully tripped setting, which is also not physically accurate for these predictions since the trip was quite aggressive [15].

However, the general trend of noise with tunnel and tip speed is more important for this level of fidelity, and the BPM model predicts these trends with an acceptable level of fidelity. The trend observed for all three proprotors is that, as the tunnel speed increases, the broadband data and predictions decrease in amplitude due to an increase in induced velocity and a reduction in blade station angles of attack. The total TBL-TE noise predictions capture this general data trend well despite a 5 dB underprediction in amplitude for the C24ND proprotor blade and suggest that assuming a moderately-to-fully tripped boundary layer gives the best predictions for these limited results. Although not shown here, similar trends were observed for OPT-III and COPR-3 and the moderately tripped setting when the tunnel Mach number was held constant and the tip Mach number was varied.

3. The Variation of Boundary Layer Thicknesses with Mach Number

The need for the moderately tripped boundary layer setting suggests that the displacement thicknesses (δ^*) predicted by BPM for the untripped settings are too small for the boundary layers encountered in the experimental setup. Although it is possible that additional 3D flow effects could influence the boundary layer thickness in the experiments, a more likely explanation is that the trip setting relates to exceeding the Mach number limit of the BPM model (see Fig. 4).

To investigate this Mach number deficiency, XFOIL was used to compute boundary layer thicknesses for an NACA 0012 airfoil. For a range of angles of attack, the freestream Mach number was varied while Reynolds number was held constant and the boundary layer thicknesses were extracted. Increasing the Mach number while maintaining a constant Reynolds number effectively reduces the chord. The airfoil was simulated at a freestream chord-based Reynolds number (Re_c) of 500,000 and for four Mach numbers: 0.1, 0.2, 0.4, and 0.6. The Mach = 0.6 condition represents the approximate flow quantities at 90% blade span for the C24ND proprotor operating at a tip Mach number of 0.667. The XFOIL calculations were performed with the e^N transition method. A critical amplification factor of N_{crit} = 9 was used, which corresponds to a freestream turbulence intensity (FSTI) of 0.07% [23].

Figure 13 shows the extracted suction-side boundary layer displacement thicknesses normalized by chord, δ_s^*, plotted against angle of attack for the four Mach numbers. The untripped, moderately tripped, and fully tripped displacement thicknesses modeled by BPM for the same Reynolds number are plotted for comparison. The BPM method assumes δ^* is invariant to Mach number, so only one set of curves is shown. The general trend is that at low Mach numbers, the displacement thicknesses are relatively Mach-number independent and appear well modeled by the untripped BPM

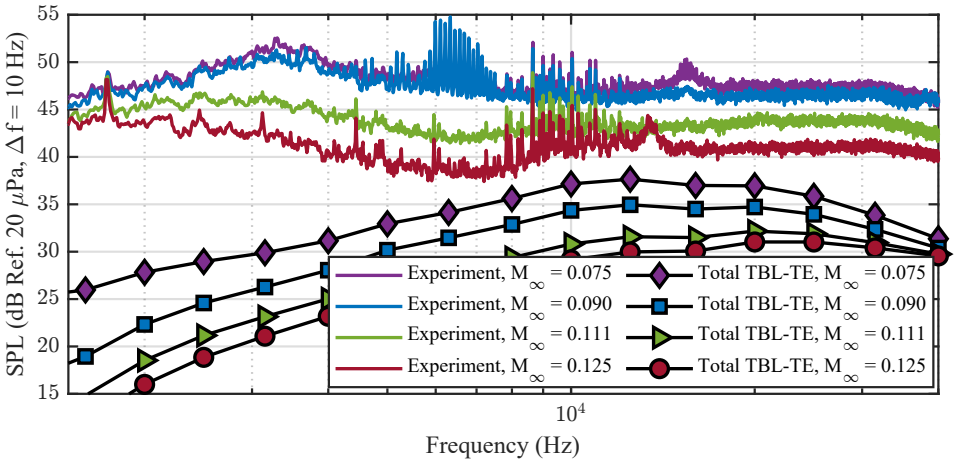

(a) Untripped Boundary Layer

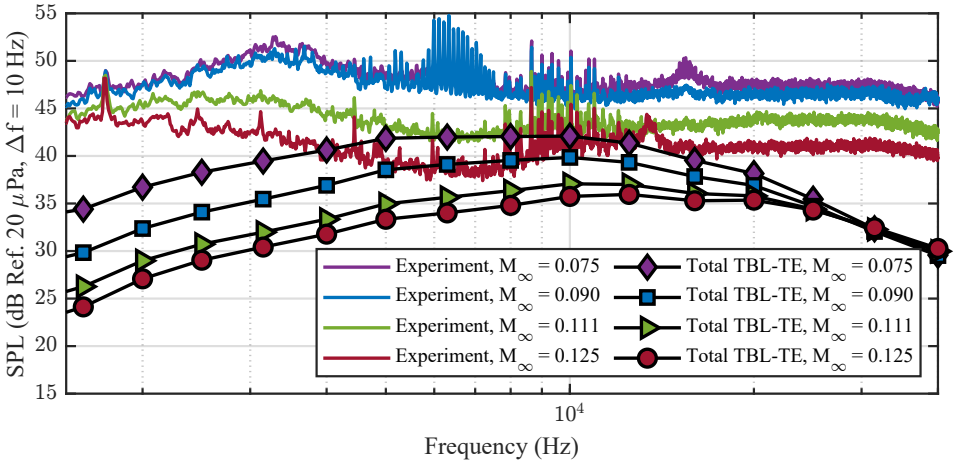

(b) Moderately Tripped Boundary Layer

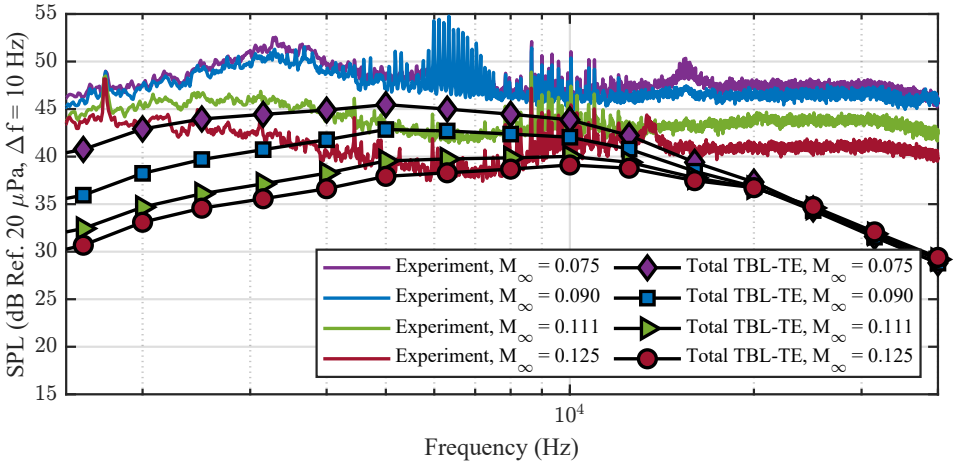

(c) Fully Tripped Boundary Layer

Fig. 10 The effect of varying freestream velocity and boundary layer trip setting on Total TBL-TE predictions for the C24ND proprotor operating at M_{tip} = 0.667. Experimental narrowband (10 Hz) data are shown by solid colored lines. Predictions are shown in black lines with symbols.

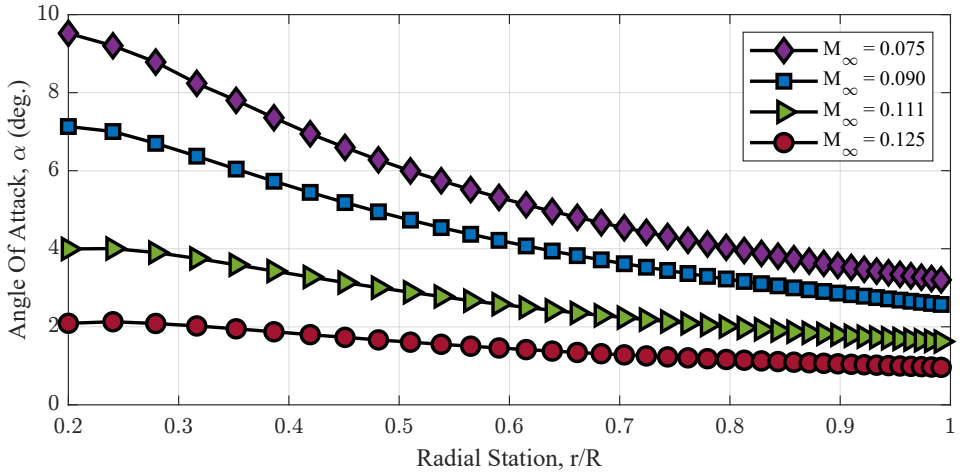

Fig. 11 Angles of attack predicted by PAS for the C24ND proprotor at M_{tip} = 0.667 varying tunnel speeds (M_∞).

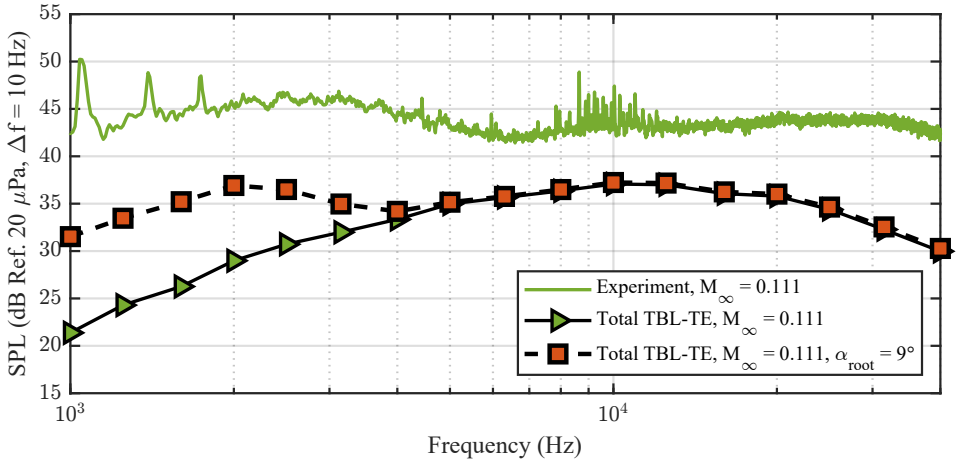

Fig. 12 Modeling additional root stall noise for the C24ND proprotor at M_{tip} = 0.667 and M_∞ = 0.111.

curve. However, for Mach = 0.4 and Mach = 0.6, the displacement thicknesses diverge from the untripped BPM curve and trend toward the fully tripped BPM curve at higher angles of attack.

Although the XFOIL predictions are likely questionable at the highest angles of attack due to the possibility of flow separation, Fig. 13 does suggest that for the OPT-III and C24ND, both of which operate with tip speeds above Mach = 0.6, the moderately tripped or fully tripped curves might give better predictions for δ^* by increasing the boundary layer thicknesses over the too-thin boundary layers predicted by the untripped setting. This gives some justification for using these settings in the previous section. Figure 13 also suggests that δ^* could vary with Mach number, which was not considered in the BPM model.

To better demonstrate the issue, Figure 14 shows the δ_s^* for each of the four Mach numbers as a ratio to the δ_s^* from the Mach = 0.1 case. This suggests that a correction factor of 2–4 times δ_s^* might be appropriate for proprotors operating at high tip Mach numbers. If such a correction is implemented, however, it should also vary with angle of attack. This gives some incentive to investigate boundary layer characteristics further for these blades.

B. Bluntness Vortex Shedding Noise

The second of the two broadband noise sources investigated in this work is BVS noise, which is due to vortices being shed from a blunt trailing edge. In addition to aerodynamic quantities (M, Re, and δ_{avg}^*), bluntness vortex shedding also depends on two geometric parameters: h, the thickness of the blunt trailing edge, and Ψ, the trailing edge closure angle

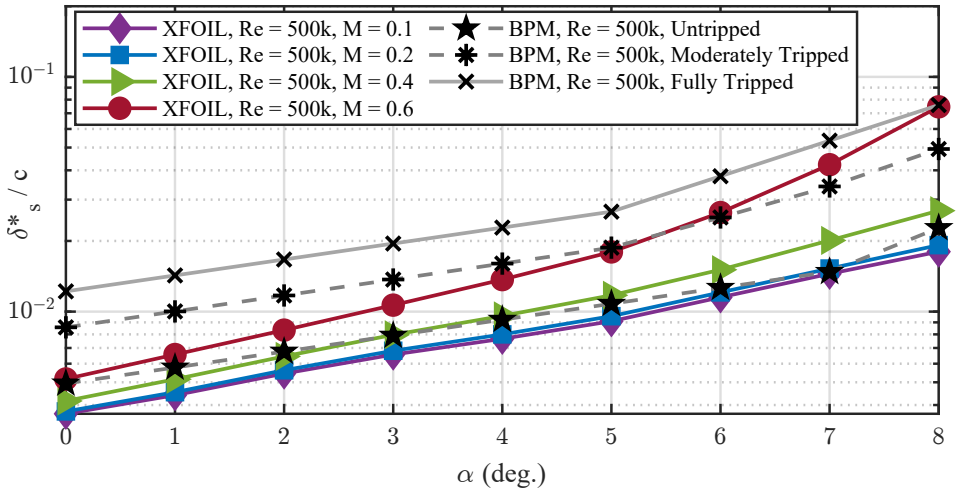

Fig. 13 Effect of Mach number on suction side boundary layer displacement thicknesses (δ^*_s) as a function of angle of attack for an NACA 0012 airfoil operating at a constant chord-based Reynolds number, Re_c = 500,000. XFOIL predictions are shown in solid color lines and BPM predictions are shown in gray lines, both for untripped boundary layers.

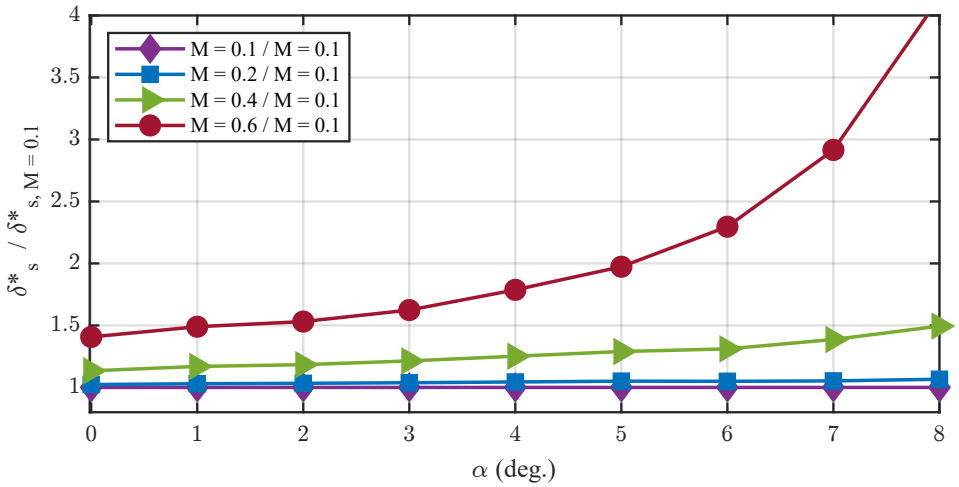

Fig. 14 The ratio of suction side boundary layer displacement thicknesses (δ^*_s) to δ^*_s calculated for Mach = 0.1. All boundary layer thicknesses computed in XFOIL at Re_c = 500,000.

(see the diagram in Fig. 15). Notably, this noise source is not dependent on α. This section investigates various settings for h and Ψ and studies BVS predictions for all three proprotors. Additionally, a dependence of BVS noise on angle of attack, α, is investigated.

1. Tuning Trailing Edge Geometry Properties

Focusing first on the OPT-III proprotor, various values of the h and Ψ parameters were investigated to determine their influence on BVS predictions. The parameter h is the trailing edge thickness, in meters. For these predictions, it is assumed that h is a constant percentage of the airfoil chord at a given blade station. Therefore, the trailing edge thickness is given as h/c, the ratio of h to the chord, c and is shown as a percentage. The parameter Ψ, the trailing edge closure angle, is given in degrees. For an NACA 0012, the measured value for Ψ is 14° [15].

Using the moderately tripped setting, BVS predictions for the OPT-III proprotor at M_{tip} = 0.619 and M_∞ = 0.111 were made for three values of h (1.0%, 1.75%, and 2.25%) and three values of Ψ (7.0°, 10.5°, and 14.0°). Figure 16 shows these bluntness predictions compared to the experimental data at the same flow condition. The total TBL-TE

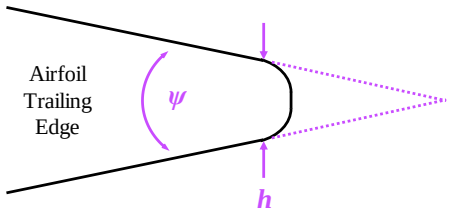

Fig. 15 Trailing edge geometry inputs, h and Ψ, for the BVS noise model.

prediction is included for reference to see where the TBL-TE spectra falls off and where bluntness noise is expected to be found.

The predictions in Fig. 16 show that BVS noise occupies a narrower range of frequencies than TBL-TE noise and that this source occurs at higher frequencies. In general, increasing the trailing edge thickness (h/c) shifts the BVS spectral peak lower in frequency and higher in amplitude. Increasing the trailing edge closure angle (Ψ) primarily increases the amplitude of the BVS peak, but also shifts the peak frequency slightly higher.

The best prediction is given by the settings $h/c = 1.75\%$ and $\Psi = 7°$, which matches the bluntness peak between 30 kHz and 40 kHz observed in the experimental data. Limited measurements made along the blades of the experimental test articles suggested that using $h/c = 1\%$ to 3% is appropriate. Additionally, the trailing edge thicknesses are reasonable given previous predictions [12]. However, the fact that Ψ had to be reduced from the physical value of 14° to 7° to match the BVS amplitude indicates that the BVS model is not accounting for the trend in δ^* correctly.

Identifying one set of h/c and Ψ for all predictions was the ideal goal. However, no such set of parameters was found to give good predictions over a range of tunnel and tip speeds for all three proprotors. For each proprotor, a constant value of h/c was found that gave good predictions, but this parameter differed between proprotors. The quantity Ψ had to be tuned on a case-by-case basis for each BVS prediction. This is illustrated in Fig. 17, which shows the best predictions for each proprotor at the design condition ($M_\infty = 0.111$). The moderately tripped boundary layer setting was used, and the total TBL-TE (green triangles) and BVS (purple squares) components are shown along with the total broadband (BB) predictions (gray circles). The experimental data for each case are also shown in gray lines. For the COPR-3 case, the tunnel background is also included as a reminder of the low signal-to-noise ratio of the measured data.

The BVS noise for the OPT-III and C24ND proprotors covers a narrower frequency range when compared to the BVS noise for the COPR-3 proprotor blade. This is likely due, in part, to the tapering chord of the COPR-3. In contrast, the C24ND and OPT-III proprotors have approximately constant chords. The frequency of broadband noise emitted by a given blade station relates to both the velocity and the chord length. Assuming a constant velocity scale, different chord lengths (and different dimensional trailing edge bluntnesses) would result in different length scales, hence different frequencies in the radiated noise. Therefore, a tapering chord would likely spread out the BVS noise over a wider range of frequencies than for a constant chord.

Another possibility is that bluntness noise is a function of Mach number as predicted by Brooks, Pope, and Marcolini [15], who suggested that BVS noise did not occur at section Mach numbers over 0.45. The outer portion of the C24ND and OPT-III blades do not generate BVS noise because of the high proprotor tip speed and high section Mach numbers, leaving more of a pronounced BVS peak with a quick fall off at high frequencies.

For all three predictions, the total TBL-TE and BVS peaks align well with the frequency content of the experimental spectra. A dip is observed in the broadband predictions where the TBL-TE noise transitions to BVS noise. This dip suggests the possibility that even if the peak amplitudes and frequencies are well predicted for TBL-TE and BVS noise, the spectral shapes may not always be well predicted for nonpeak frequencies.

The amplitudes of both TBL-TE and BVS noise agree well for the OPT-III and COPR-3, but there is a 10 dB underprediction for the C24ND proprotor, possibly due to the proprotor high tip Mach number (see Section III.A.3). For the OPT-III proprotor, the best predictions were found with $h/c = 1.75\%$ and $\Psi = 7°$. For the C24ND proprotor, the best predictions were found with $h/c = 1.75\%$ and $\Psi = 14°$ despite the almost 10 dB underprediction in amplitude. For the COPR-3 proprotor, the best predictions were found with $h/c = 1.0\%$ and $\Psi = 9°$. All predictions drop off at the highest frequencies (above 70 kHz).

Although a constant h/c and Ψ could not be found that yielded good BVS predictions for all proprotors and flight conditions, when the parameters were tuned, the BVS predictions matched well with the experimental data. The variation in trailing edge thicknesses are reasonable given that all proprotors have approximately the same physical trailing edge

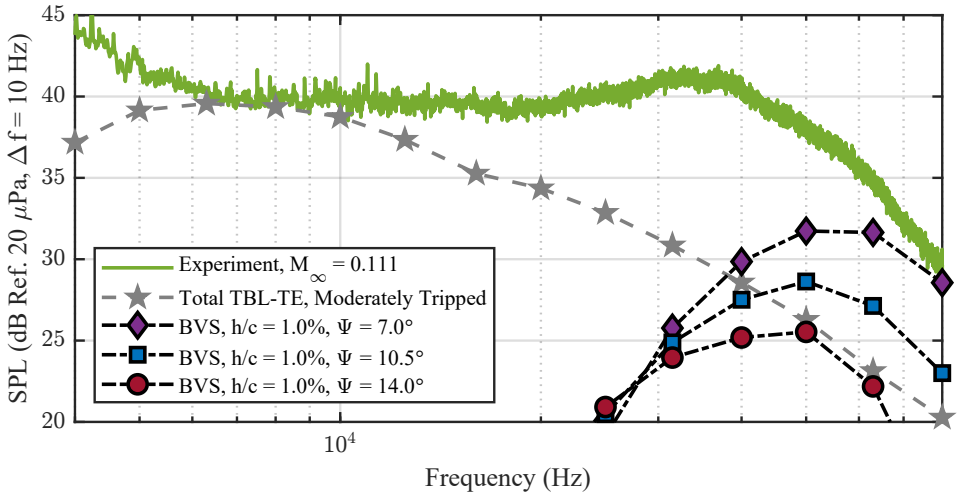

(a) h/c = 1.0%

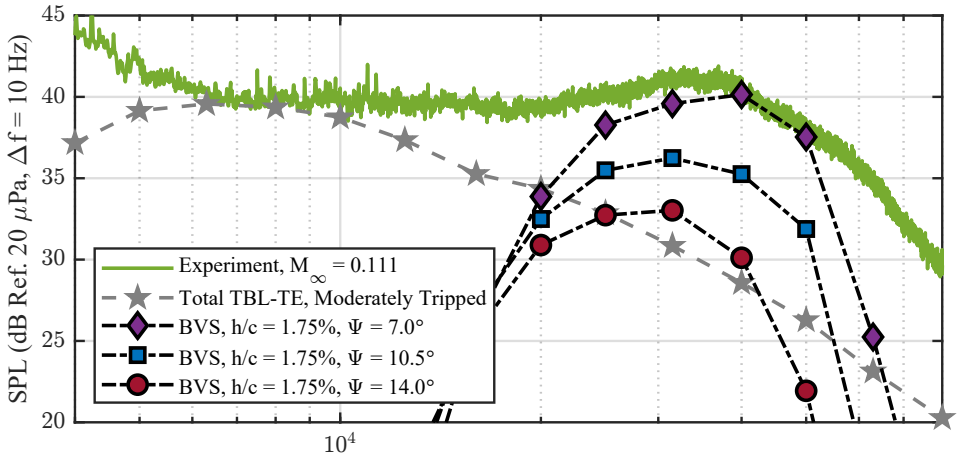

(b) h/c = 1.75%

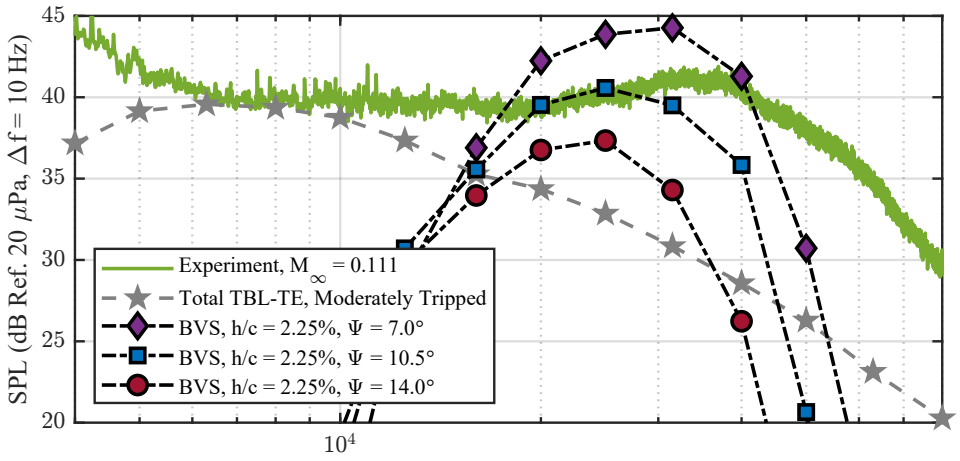

(c) h/c = 2.25%

Fig. 16 The effect of varying h/c and Ψ on BVS noise for the Opt-III proprotor at M_{tip} = 0.619 and M_∞ = 0.111. Experimental narrowband (10 Hz) data are shown with predictions of Total TBL-TE. BVS predictions are shown by the black lines with symbols.

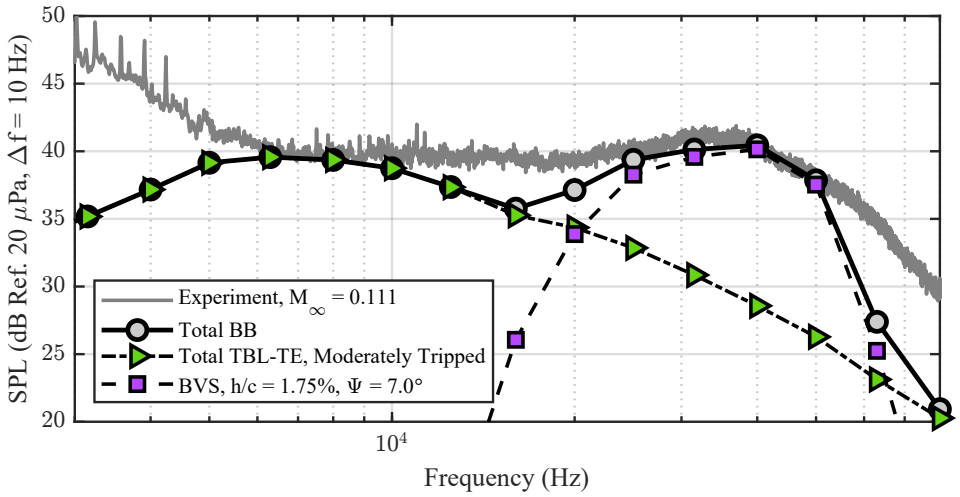

(a) OPT-III proprotor at M_{tip} = 0.619

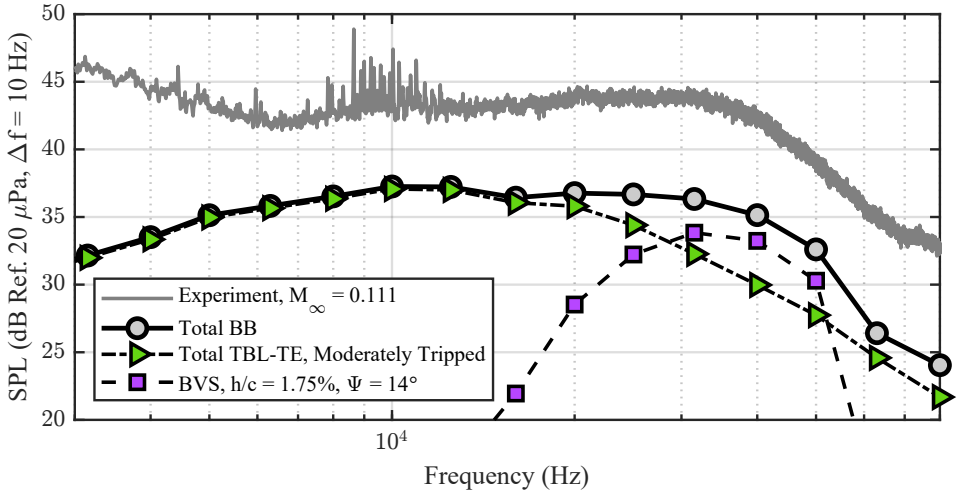

(b) C24ND proprotor at M_{tip} = 0.667

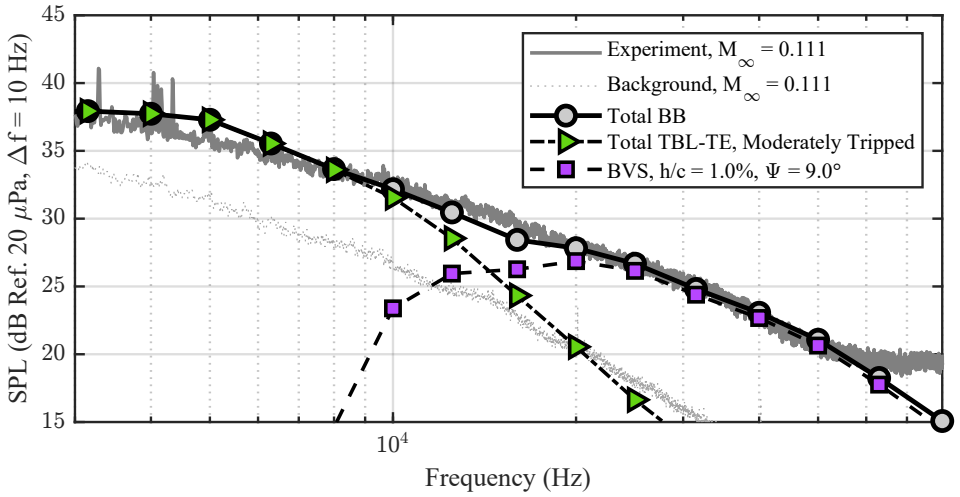

(c) COPR-3 proprotor at M_{tip} = 0.343

Fig. 17 Total broadband noise, Total TBL-TE, and BVS noise predictions for the all three proprotors at M_∞ = 0.111, the design flight condition.

thickness. The OPT-III and C24ND required the same h/c, 1.75%, which makes sense because their chord lengths are similar. The COPR-3 proprotor needed a smaller h/c, 1.0%, which also makes sense given that the chord lengths are much larger than either the OPT-III or C24ND blades. The large changes in Ψ between each case suggests that the BVS model is incomplete. A possible explanation is that bluntness noise varies with an additional parameter, such as angle of attack.

2. Influence of Angle of Attack

In the bluntness noise study [24] cited by the BPM report, the effect of α on BVS was not explicitly considered, probably because the authors could not separate bluntness noise from the other trailing edge noise sources for an airfoil at an angle of attack. In the BPM report, they modeled bluntness noise at an angle of attack of zero degrees for a symmetric NACA 0012 airfoil. The BVS model has an implicit dependence on angle of attack because it is based on δ^*_{avg}, the average of the suction-side displacement thickness, δ^*_s, and pressure-side displacement thickness, δ^*_p. As α increases, δ^*_s and δ^*_p increase with angle of attack but have different trends [15]. It is possible that the average of δ^*_s and δ^*_p does not adequately reflect how δ^* (and BVS noise) varies with α.

Additionally, it is likely that the coherent vortex shedding that leads to BVS noise could be altered, disrupted, or enhanced by a change in angle of attack. Given that h/c and Ψ had to be tuned on a case-by-case basis in the previous section, it is reasonable to assume that the BVS noise model is either incorrect or is missing a contributing factor. The possibility that BVS noise varies with α is investigated in this section by looking at predictions for the OPT-III proprotor at a fixed tip Mach number and at three increasing tunnel speeds.

Predictions of total broadband (BB) noise for the OPT-III proprotor at $M_{tip} = 0.619$ and three tunnel speeds are plotted and compared to the experimental data in Fig. 18. All predictions are performed with $h/c = 1.75\%$. Figure 18 (a) shows predictions with Ψ set to 14°. This leads to BVS noise (15 kHz to 80 kHz) that increases with increasing tunnel speed, which is the opposite trend observed in the experimental data. Figure 18 (b) shows predictions where Ψ is tuned for each case. The tuning was performed by manually adjusting Ψ until the spectral shape and amplitudes of the BVS noise visually matched the experimental data. With adjusted values of Ψ, the BVS noise does capture the correct trends. For the fastest tunnel speed, $M_\infty = 0.125$, there is an underprediction of amplitude of several dB, but the spectral trends are correct. All three predictions have a dip in the spectra where the total TBL-TE noise transitions to BVS noise.

It should be noted that in order to match the BVS noise for the $M_\infty = 0.090$ case, Ψ was set to 1°, which is approximately a flat plate. For the $M_\infty = 0.125$ case, Ψ was set to 12°, which is close to the value for an NACA 0012. In other words, the parameters go from modeling BVS noise for an NACA 0012 airfoil with a boat tail to modeling BVS noise for a flat plate, which is quite a significant change.

The plots in Fig. 18 demonstrate further that BVS could vary with angle of attack since the only quantities that change between the three flight conditions are the effective Mach number at each blade station and the effective angle of attack. The BVS model already varies with Mach number, so the only remaining quantity is angle of attack. Figure 19 shows the angles of attack for these three tunnel speeds. As the tunnel speed increases, the angle of attack decreases as expected. For the predictions, Ψ moves toward the measured value of 14° as the angles of attack move toward zero, which suggests that Ψ should deviate less from the measured value the closer the blade station angles of attack are to 0°.

Finally, BVS predictions for flight conditions with the same angle of attack distribution should be able to use the same values of h/c and Ψ if BVS really does vary with angle of attack. A proprotor operating at the same advance ratio, J, but different tip and tunnel speeds should have the same α distribution along the blade.

Figure 20 shows two COPR-3 flight conditions at a constant advance ratio ($J = 0.94$) and the corresponding total broadband noise predictions. For operating conditions of $M_{tip} = 0.30$ and $M_\infty = 0.090$, the BVS noise source was tuned with the parameters $h/c = 1\%$ and $\Psi = 6.5°$ for a moderately tripped boundary layer setting. The same parameters were applied to the operating conditions of $M_{tip} = 0.25$ and $M_\infty = 0.075$. Both predictions show excellent agreement for the entire broadband spectra, including the BVS noise above 10 Hz. This shows that when the α distribution is identical between two flight conditions, the BVS parameters do not need to be retuned.

Similarly, for the OPT-III proprotor at a constant advance ratio ($J = 0.56$), two predictions are made with the moderately tripped boundary layer setting and trailing edge parameters $h/c = 1.75\%$ and $\Psi = 7°$. The experimental data and predictions are shown in Fig. 21 and both agree well for the entire broadband spectra. For the operating condition $M_{tip} = 0.50$ and $M_\infty = 0.090$, an overprediction of several dB is observed for the BVS noise above 40 kHz. The general spectral shapes are matched in Fig. 21, which again indicates that if the α distribution is the same, the BVS source does not need to be retuned.

The results presented in this section demonstrate that the BVS model is incomplete and does not trend correctly with

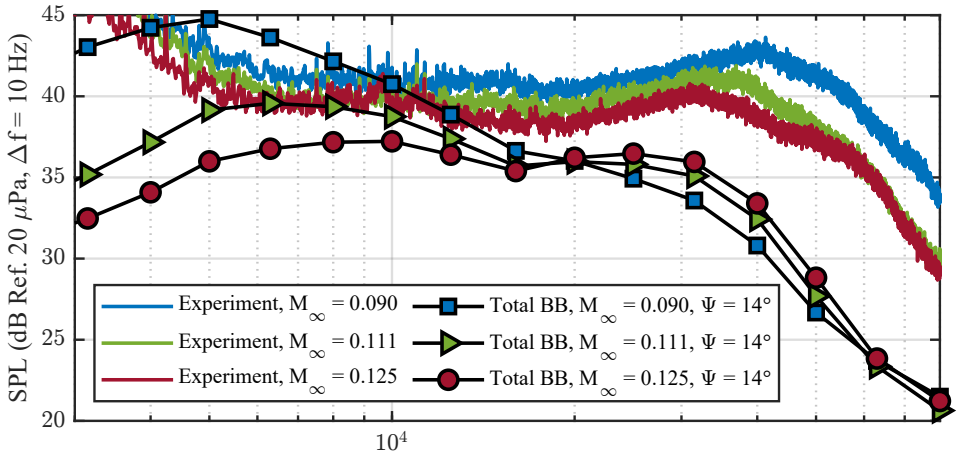

(a) Ψ = 14°

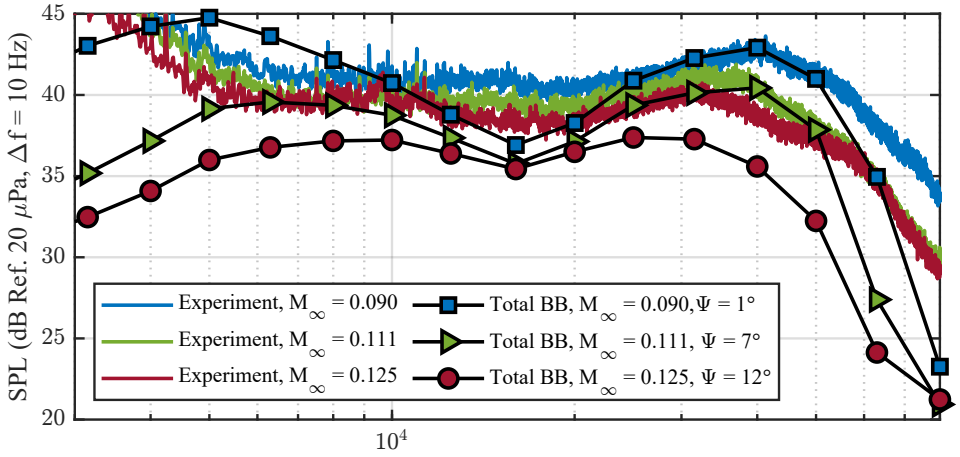

(b) Ψ Tuned for Each Condition

Fig. 18 Total broadband predictions with a constant Ψ and a Ψ tuned for each condition for the Opt-III proprotor at M_{tip} = 0.619 and varying tunnel speeds. Experimental narrowband (10 Hz) data are shown in the solid colored lines. BVS predictions using $h/c = 1.75\%$ are shown by the black lines with symbols.

angle of attack. Figures 18, 20, and 21 help make a strong case that the BVS model needs an additional dependence on angle of attack or that the BVS source varies with angle of attack. Updating the BVS model will likely eliminate having to tune the trailing edge parameters for each proprotor and flight condition.

C. Implications for Design Optimization

Predicting the correct general broadband noise trends for a range of tunnel and tip speeds is more important for the level of fidelity needed in design optimization than exactly matching experimental data. The PAS-ASNIFM model predicts these trends with an acceptable level of fidelity for TBL-TE noise. The trend observed for all three proprotors is that, as the tunnel speed increases, the broadband data and predictions decrease in amplitude due to an increase in induced velocity and a reduction in blade station angles of attack. The total TBL-TE noise predictions capture this general data trend well despite a 5 dB amplitude underprediction for the C24ND proprotor blade.

Including broadband predictions in design optimization studies requires first identifying optimal parameter settings for the BPM model since adjusting the parameters during an optimization is not ideal. From the results presented in the previous sections, the total TBL-TE noise trends were predicted well using the moderately tripped setting across

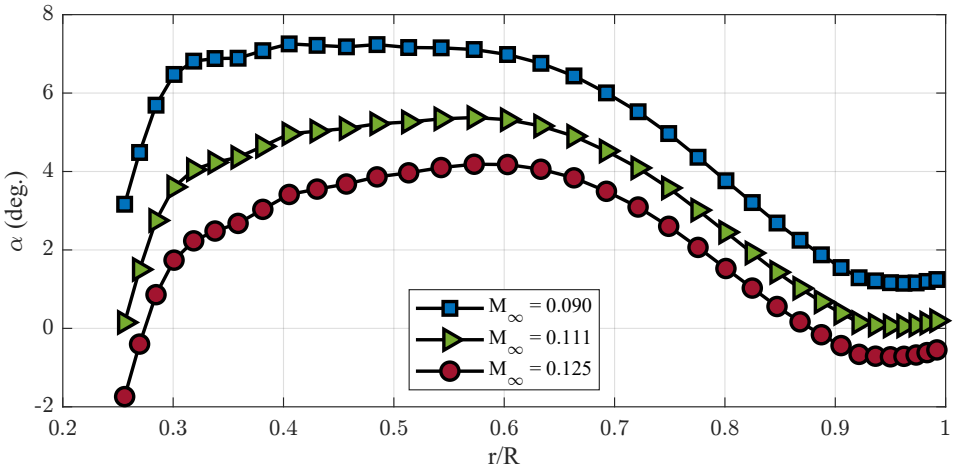

Fig. 19 Angles of attack predicted by PAS for the OPT-III proprotor at M_{tip} = 0.619 and varying tunnel speeds.

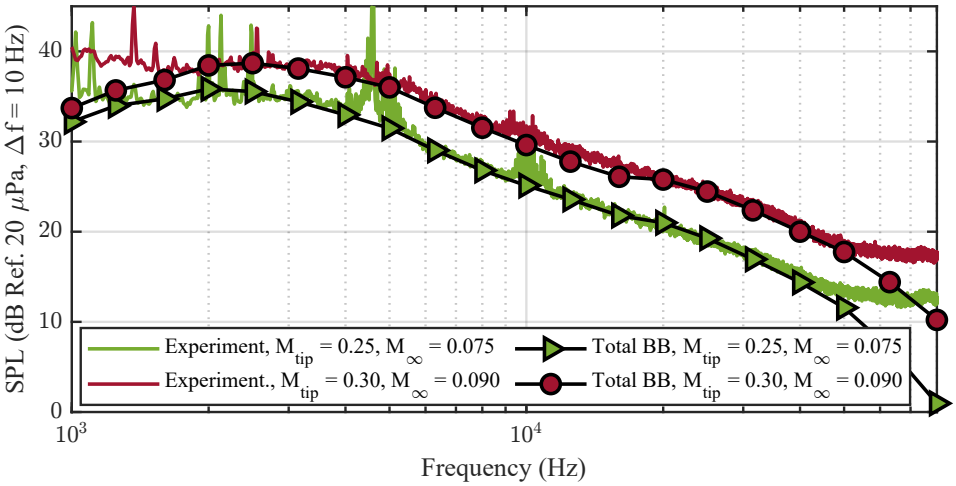

Fig. 20 Total broadband noise predictions at a constant advance ratio (J = 0.94) for the COPR-3 proprotor.

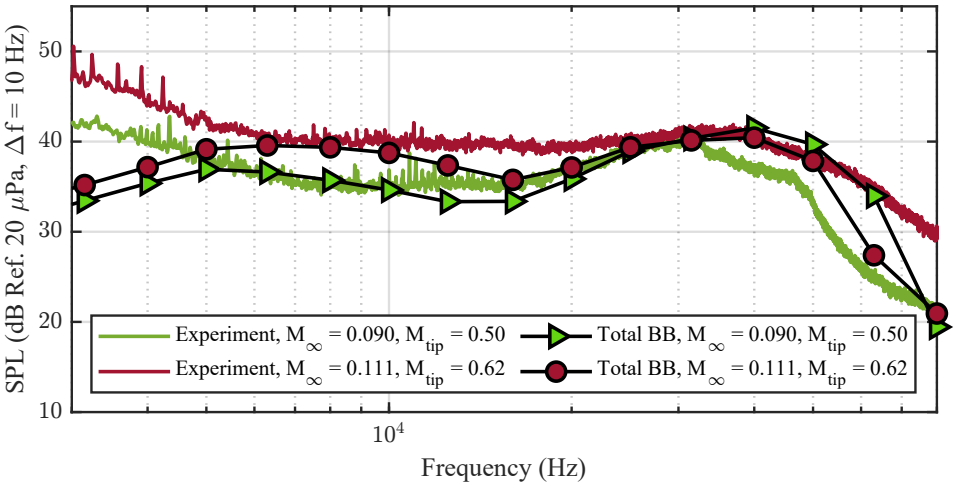

Fig. 21 Total broadband noise predictions at a constant advance ratio (J = 0.56) for the OPT-III proprotor.

multiple flight conditions for these proprotors. While it is possible that the trip setting giving the "best" prediction could change with tip or tunnel Mach number, future optimization studies on similar proprotors could likely use the same settings for a first approximation of TBL-TE noise.

Experimental data and predictions from Fig. 17 are replotted together in Fig. 22 (a) to better demonstrate trends between the three proprotors at their design conditions. Broadband predictions are shown with all noise sources except LBL-VS noise. Predictions for the C24ND proprotor were increased in amplitude by 6 dB in Fig. 22 given the underprediction observed in Fig. 17 (b). The experimental data show a reduction in broadband noise for the OPT-III proprotor compared to the baseline C24ND proprotor, while the COPR-3 proprotor shows a further noise reduction compared to the OPT-III proprotor. With the correction in amplitude, all predictions show similar trends to the experimental data and match the frequency content and spectral shapes well. Below 5 kHz, the experimental data for the C24ND and OPT-III proprotors show the existence of an additional noise source that the models cannot predict, such as root or hub noise.

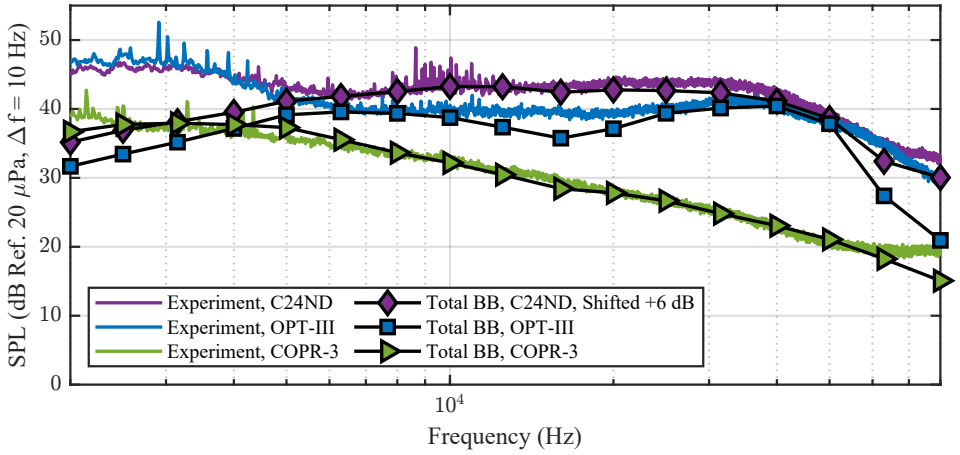

(a) Experimental Data and All Broadband Noise Components

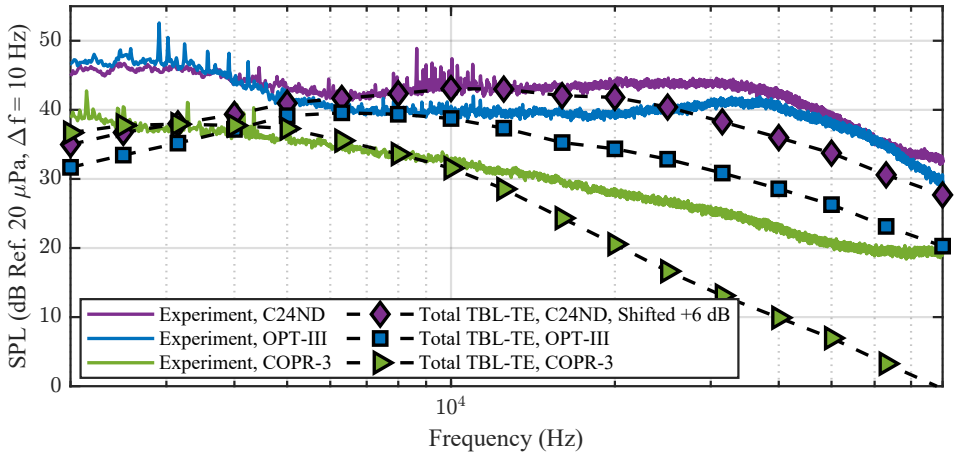

(b) Experimental Data and Total TBL-TE Noise

Fig. 22 Broadband prediction trends for the C24ND, OPT-III, and COPR-3 proprotors at their design condition, M_∞ = 0.111 and M_{tip} = 0.667, 0.619, and 0.343, respectively. Experimental narrowband (10 Hz) data are shown in the solid colored lines. Predictions are shown by lines with symbols. The C24ND predictions are shifted by 6 dB.

One additional difficulty for design optimization is the underprediction in amplitude for the C24ND proprotor observed in Fig. 17 (b). Since this was the baseline proprotor, starting with an underprediction in broadband noise amplitude causes an issue when trying to reduce the noise via an optimization process. If the noise is already low, there is nowhere for the optimizer to go or the noise reduction will be seen as minimal compared to the baseline case.

Since BVS noise required tuning the trailing edge angle, Ψ, on a case-by-case basis, it is recommended that BVS not be predicted in optimization efforts until the model is expanded to include the effects of angle of attack on BVS noise. Only including TBL-TE noise will lead to an underprediction of high frequencies where BVS should be, but since TBL-TE noise is typically the dominant broadband noise source in terms of amplitude, this is an acceptable first-order approximation for design optimization. To demonstrate the impact of predictions using only TBL-TE noise, Fig. 22 (b) shows predictions at the design condition for each proprotor and using only the total TBL-TE noise component. Figure 22 (b) shows that the general trends of the total broadband noise are still captured by only including TBL-TE noise but that roll-off of high frequencies should be expected if BVS noise is not included. Using only total TBL-TE noise might be acceptable if an integrated metric such as overall sound pressure level (OASPL) is used as part of a design optimization objective function.

If BVS is included, then using the physically measured trailing edge thickness and the physical Ψ value of 14° is recommended with the caveat that this will likely lead to an underprediction of BVS amplitudes for most flight conditions.

IV. Conclusions/Summary

For proprotors in axial forward flight, a low-fidelity toolchain using the BPM method implemented in ASNIFM was evaluated and compared to experimental data from a recent LSAWT test [17] for three proprotors operating over a range of tip and tunnel Mach numbers. Two dominant self-noise broadband sources, total TBL-TE and BVS noise, were investigated.

For total TBL-TE noise, the general trends were matched well by the BPM model for a moderately tripped boundary layer despite the fact that the blades were operating without a physical trip. It was hypothesized that the reason for needing to artificially trip the boundary layer in these predictions was that the increased tip Mach number for these proprotors leads to a thicker boundary layer in the experiments than BPM predicts for an untripped boundary layer. By increasing the trip setting, this increased the boundary layer thicknesses (mainly δ^*) in the predictions and adjusted the peak TBL-TE noise frequency and amplitude. The amplitudes for TBL-TE noise were not always predicted well (i.e., for the C24ND proprotor). The discovery of a possible dependence of δ^* on Mach number, which was not considered in the original BPM models for δ^*, indicates that the TBL-TE model needs to be developed further. Additionally, the best trip setting for a single TBL-TE prediction might vary between proprotors and flight conditions since the boundary layer thickness behavior might vary as well.

For BVS noise, the trailing edge geometries had to be tuned for each flight condition. Once tuned, the BVS noise model predicted the correct broadband trends. However, tuning BVS for each prediction is impractical without the presence of experimental data. It was hypothesized that the BVS model required tuning because it is incomplete and needs an additional dependence on angle of attack. Additionally, the BVS noise source itself might vary with angle of attack, which was not investigated in the original BPM report. Predictions at a constant advance ratio (same angle of attack distribution) agreed well for BVS noise without requiring retuning of the trailing edge geometries, which strengthens the argument that BVS noise should vary with angle of attack.

Future work will focus on evaluating how the BPM-based predictions model the directivities of TBL-TE and BVS noise sources, as well as how these two broadband sources contribute to integrated noise metrics like OASPL. Making use of a higher-fidelity aerodynamics solver that incorporates radial corrections or stall delay might improve both the blade station aerodynamics and the broadband predictions. Settings for the LBL-VS and tip vortex formation noise sources also need to be studied further, as well as investigating possible hub or root stall noise. Ultimately, improving the BPM self-noise method is the next step.

Expanding the BPM models for both noise sources will likely require a combination of experimental and high-fidelity computational investigations. For instance, source localization techniques may be necessary to determine where certain self-noise sources and frequencies are generated along the proprotor blade span. Measurements of the boundary layer thicknesses for different airfoils, surface roughnesses, and Mach numbers would assist with developing a more complete TBL-TE model. Investigating the coherence of surface fluctuations and how they relate to the radiated noise and vortices shed off the trailing edge [24] could inform on how BVS noise may change with angle of attack.

Improving low-fidelity broadband prediction tools will lead to more accurate isolated proprotor and full vehicle broadband noise predictions, potentially leading to the inclusion of broadband noise into the UAM vehicle design process. Both are a small step toward designing quiet vehicles for UAM operations.

Acknowledgments

The authors thank the NASA Transformational Tools and Technology (TTT) project for funding and supporting this work. The authors also thank Nicole Pettingill for providing insight into the broadband predictions.

References

[1] Garrow, L. A., German, B., Schwab, N. T., Patterson, M. D., Mendonca, N., Gawdiak, Y. O., and Murphy, J. R., "A Proposed Taxonomy for Advanced Air Mobility," AIAA Paper 2022-3321, AIAA AVIATON 2022 Forum, Chicago, Illinois, June, 2022. doi:10.2514/6.2022-3321.

[2] Rizzi, S. A., Huff, D. L., Boyd, Jr., D. D., Bent, P., Henderson, B. S., Pascioni, K. A., Sargent, D. C., Josephson, D. L., Marsan, M., He, H., and Snider, R., "Urban Air Mobility Noise: Current Practice, Gaps, and Recommendations," NASA TP–2020-5007433, National Aeronautics and Space Administration, October 2020.

[3] Silva, C., Johnson, W. R., Solis, E., Patterson, M. D., and Antcliff, K. R., "VTOL Urban Air Mobility Concept Vehicles for Technology Development," AIAA Paper 2018-3847, AIAA AVIATION 2018 Forum, Atlanta, Georgia, June 2018. doi:10.2514/6.2018-3847.

[4] Bain, J., Goetchius, G., and Josephson, D., "Flyover Noise Comparison Between Joby Aircraft and Similar Aircraft," VFS 78th Annual Forum & Technology Display, Fort Worth, Texas, May 2022. doi:10.4050/F-0078-2022-17437.

[5] Pascioni, K. A., Watts, M. E., Houston, M., Lind, A., Stephenson, J. H., and Bain, J., "Acoustic Flight Test of the Joby Aviation Advanced Air Mobility Prototype Vehicle," AIAA Paper 2022-3036, 28th AIAA/CEAS Aeroacoustics Conference, Southampton, United Kingdom, June 2022. doi:10.2514/6.2022-3036.

[6] Gray, J. S., Hwang, J. T., Martins, J. R. R. A., Moore, K. T., and Naylor, B. A., "OpenMDAO: an open-source framework for multidisciplinary design, analysis, and optimization," *Structural and Multidisciplinary Optimization*, Vol. 59, No. 4, 2019, pp. 1075–1104. doi:10.1007/s00158-019-02211-z.

[7] Leishman, J. G., *Principles of Helicopter Aerodynamics*, Cambridge Aerospace Series, Cambridge University Press, 40 West 20th St., New York, New York, 10011-4211, 2000.

[8] Lopes, L. V., and Burley, C. L., "ANOPP2 User's Manual," NASA TM 2016-219342, National Aeronautics and Space Administration, October 2016.

[9] Ingraham, D., Gray, J. S., and Lopes, L. V., "Gradient-Based Propeller Optimization with Acoustic Constraints," AIAA Paper 2019-1219, AIAA SciTech Forum, San Diego, California, January 2019. doi:10.2514/6.2019-1219.

[10] Zawodny, N. S., Boyd, Jr., D. D., and Burley, C., "Acoustic Characterization and Prediction of Representative, Small-Scale Rotary-Wing Unmanned Aircraft System Components," AHS International 72nd Annual Forum & Technology Display, West Palm Beach, Florida, May 2016.

[11] Pettingill, N. A., and Zawodny, N. S., "Identification and Prediction of Broadband Noise for a Small Quadcopter," VFS International 75th Annual Forum & Technology Display, Philadelphia, Pennsylvania, May 2019.

[12] Pettingill, N. A., Zawodny, N. S., Thurman, C., and Lopes, L. V., "Acoustic and Performance Characteristics of an Ideally Twisted Rotor in Hover," AIAA Paper 2021-1928, AIAA SciTech Forum, Virtual, January 2021. doi:10.2514/6.2021-1928.

[13] Thurman, C., Zawodny, N. S., Pettingill, N. A., Lopes, L. V., and Baeder, J. D., "Physics-informed Broadband Noise Source Identification and Prediction of an Ideally Twisted Rotor," AIAA Paper 2021-1925, AIAA SciTech Forum, Virtual, January 2021. doi:10.2514/6.2021-1925.

[14] Nguyen, L. C., and Kelly, J. J., "A Users Guide for the NASA ANOPP Propeller Analysis System," NASA CR 4768, National Aeronautics and Space Administration, February 1997.

[15] Brooks, T. F., Pope, D. S., and Marcolini, M. A., "Airfoil Self-Noise and Prediction," NASA RP 1218, National Aeronautics and Space Administration, July 1989.

[16] Lee, S., Ayton, L., Bertagnolio, F., Moreau, S., Chong, T. P., and Joseph, P., "Turbulent Boundary Layer Trailing-Edge Noise: Theory, Computation, Experiment, and Application," *Progress in Aerospace Sciences*, Vol. 126, 2021, 100737. doi:10.1016/j.paerosci.2021.100737.

[17] Zawodny, N. S., Pettingill, N. A., Lopes, L. V., and Ingraham, D. J., "Experimental Validation of an Acoustically and Aerodynamically Optimized UAM Proprotor Part 1: Test Setup and Results," NASA TM-20220015637, National Aeronautics and Space Administration, February 2023.

[18] Icke, R. O., Baysal, O., Lopes, L. V., and Diskin, B., "Optimizing Proprotor Blades Using Coupled Aeroacoustic and Aerodynamic Sensitivities," AIAA Paper 2021-3037, AIAA AVIATON 2021 Forum, Virtual, August 2021. doi:10.2514/6.2021-3037.

[19] Vogeley, A. W., "Sound-Level Measurements Of A Light Airplane Modified To Reduce Noise Reaching The Ground," NACA TR 926, National Advisory Committee for Aeronautics, January 1949.

[20] Theodorsen, T., "Theory of Wing Sections of Arbitrary Shape," NACA TR 411, National Advisory Committee for Aeronautics, January 1931.

[21] Theodorsen, T., and Garrick, I. E., "General Potential Theory of Arbitrary Wing Sections," NACA TR 452, National Advisory Committee for Aeronautics, January 1940.

[22] Thurman, C. S., Pettingill, N. A., and Zawodny, N. S., "The Effect of Boundary Layer Character on Stochastic Rotor Blade Vortex Shedding Noise," VFS 78th Annual Forum & Technology Display, Fort Worth, Texas, May 2022. doi: 10.4050/F-0078-2022-17428.

[23] Mack, L. M., "Transition Prediction and Linear Stability Theory," 1-1-1-22 of AGARD 1977.

[24] Brooks, T. F., and Hodgson, T. H., "Trailing Edge Noise Prediction from Measured Surface Pressures," *Journal of Sound and Vibration*, Vol. 78, No. 1, 1981, pp. 69–117. doi:10.1016/S0022-460X(81)80158-7.